BULLETIN OF THE POLISH ACADEMY OF SCIENCES
TECHNICAL SCIENCES, Vol. 74(2), 2026, Article number: e157320
DOI: 10.24425/bpasts.2026.157320

Modal analyses of nonuniform axially functionally graded Euler-Bernoulli beams

Esra Zeynep ŞENSOY* **and Tarık BARAN**

Faculty of Engineering and Natural Science, Civil Engineering Department, Osmaniye Korkut Ata University, Osmaniye, Türkiye

Abstract. The dynamic response of functionally graded beams is of immense importance in modern engineering applications where structural elements often exhibit material inhomogeneity and geometric nonuniformity. This study investigates flexural free vibrations of axially functionally graded Euler-Bernoulli beams with nonuniform cross-sections, where both geometric dimensions and material properties vary along the beam axis. The governing equations of motion were discretized and solved using the Haar wavelet method, which provides an efficient numerical scheme. Four classical boundary conditions: clamped-free, pinned-pinned, clamped-pinned, and clamped-clamped were analyzed to demonstrate the versatility of the approach. The accuracy of the method was verified by comparison with benchmark solutions available in the literature. Extended case studies were then performed for tapered and cone-shaped beams with linearly varying depth or width, considering axially functionally graded material. The results demonstrate that variations in axial cross-sectional geometry have a greater impact on natural frequencies and mode shapes than material gradation. This study revisits the Haar wavelet method and extends its application to conditions that were previously unstudied, such as different functionally graded material models in tapered and cone configurations. The validated results are in good agreement with existing literature. Finally, detailed graphs and tables present the results obtained for previously uninvestigated cases.

Keywords: Haar wavelet method; functionally graded material; functionally graded beam; nonuniform axially functionally graded beam; free vibration analysis.

1. INTRODUCTION

Functionally graded materials (FGMs) have numerous advantages as they combine the superior properties of two or more different materials and gradually change them within a structure to create more durable material or serve a specific purpose. For example, in high-temperature composites in which functionally graded (FG) metal and ceramics are used together, thermal and residual stresses due to the discontinuity between the metal-ceramic layers cause tears and cracks between the layers. Metal derived from this material pair has numerous positive characteristics, such as toughness, electrical conductivity, and machinability. Ceramics, on the other hand, have low density, high strength, and thermal resistance. The distinct advantages of using these materials, i.e., the high toughness, machinability, and bonding capabilities of metals and the corrosion and oxidation resistance of ceramics, can be combined to create continuity in the material [1–5]. Structural members with FGMs are mixed at a certain volumetric ratio, and the materials are exchanged with each other as a function of the thickness or axis of the material [6–8]. Two of the most widely recognized formulations of FG structures are the exponential law [9] and the power law [10].

Suresh and Mortensen [11] developed thermal, elastic, and plastic deformation models of staggered multilayers in the context of classical beam and plate theories, along with strategies for developing 'design diagrams' for thermomechanical performance. They also presented methods to identify the conditions governing the onset of instability and abrupt changes triggered by deformation in staggered multi-layer structures. By using FGMs, the mutual graded dispersion of the materials causes continuous change, preventing the formation of an interface in which cracks can develop between the materials, making FGMs ideal for advanced technological applications. In this regard, an intensive study on FGM structures was recently conducted [6,12,13]. In 1994, one of the first studies on beams with variable cross-sections was conducted, with Naguleswaran [14] examining a direct solution for the transverse vibration of wedge and cone Euler-Bernoulli beams with various support conditions. Bessel functions have been employed to obtain the analytical solution of the mode shape equations of graded beams. For FG beams, the gradient may be oriented in either the thickness or the axial direction [7, 15]. Reviewing the literature, it can be seen that most previous works on FG beams considered the gradation of material properties in various directions, though a modest number of researchers studied the structural behaviors of those types of FG beams in the axial direction [16]. Furthermore, there are even fewer studies on beams where material changes accompany section and mass changes. Similarly, some researchers reported that in comparison to studies on FG plates and shells [17–32], research on FG beams is relatively limited [2, 33, 34]. There are also some studies devoted to free vibration for FG beams. Sharma and Singh [35] presented a study on the free vibration analysis of axially clamped-clamped FGM beams using the generalized differential quadrature method. Following this, Tu-

*e-mail: e.z.sensoy@gmail.com

Manuscript submitted 2025-07-21, revised 2025-10-31, initially accepted for publication 2025-11-19, published in March 2026.

ran *et al.* [36] studied the free vibration and buckling analysis of FG porous beams subjected to various boundary conditions. They solved the FG porous beam analytically and compared it with the finite element and artificial neural network methods. Mao *et al.* [37] analyzed vibration and wave propagation in FGM beams with inclined cracks. They proposed a finite element method to study vibration and wave propagation in FGM beams with multiple inclined cracks by considering the local flexibility matrix caused by the cracks. Zhang *et al.* [38] proposed a multiscale numerical method to study the static, dynamic, and buckling behavior of FG beams reinforced with graphene platelets. They assumed that the beam was divided into FG layers along the thickness, while gradation along the axial direction was achieved using the proposed finite elements. Furthermore, Li *et al.* [39] developed a modified quasi-3D theory and the mixed beam element model for static analysis of FG beams, while Tang *et al.* [40] provided an exact general elasticity solution for FG rectangular beams with arbitrary distributed loads. Huang *et al.* [41] investigated the dynamic behavior of nonuniform FG beams resting on inhomogeneous foundations and subjected to moving distributed loads. They developed a numerical model to analyze the effects of material gradation, foundation heterogeneity, and load dynamics on the vibration characteristics of the beam.

Moreover, studies on axially FG beams compared to thickness direction FG beams are limited. This is because FG beams with complex governing equations are more difficult to solve precisely [42]. Sankar's work on an elasticity solution for FG beams varied the properties with the thickness of the FG beam [2]. Additionally, Sankar developed a straightforward Euler–Bernoulli type beam theory. Chakraborty *et al.* [43] examined the free vibration of an FG beam with elastic and thermal properties varying along its thickness. The thermoelastic behavior of the FG beam structure was investigated via the finite element method by considering shear deformation. Another study about the thickness direction of an FG beam is that of Lu and Chen [44]. They studied the free vibration of orthotropic FG beams with various end conditions. They presented a novel approach to determine the solution of a beam whose elastic constants and mass density could vary arbitrarily along the beam thickness direction. Aydoğdu and Taşkın [33] also investigated the free vibration of simply supported FG beams with edges. They used a Navier-type solution method to obtain the frequencies. They assumed that the modulus of elasticity varies along the direction of thickness, while all other material properties remain constant. Li [4] also found that all material properties of the FG beam were arbitrary functions along the beam thickness. Li presented a unified approach to analyze the static and dynamic behaviors of both Euler-Bernoulli and Timoshenko FG beams. Another study in which beam properties changed with beam thickness was that of Sina *et al.* [7], who investigated an analytical method for the free vibration analysis of FG beams. They developed a new beam theory for the free vibration analysis of FG beams, which is different from the traditional first-order shear deformation beam theory. One of the latest works, a study by El Khouddar *et al.* [45], investigated the geometrically nonlinear free vibrations of FG beams in a thermal environment with an analytical solution, assuming that the material properties changed continuously through the beam thickness and with temperature variations. Jena *et al.* [46] also examined the influence of thickness dependent gradation in FG micro-beams using Haar wavelet discretization method and the differential quadrature method, highlighting its computational efficiency and accuracy in micro-scale structural analyses. Subsequently, Nazmul *et al.* [47] presented an analytical solution for the vibration of bidirectional FG Euler-Bernoulli and Timoshenko nanobeams. They accepted that the characteristics of the FG nanobeam material varied along the axial and the thickness directions.

Though there are some techniques and methodologies for the analytical and computational analysis of nonuniform and axially FG beams, there is still a modest number of valid, simple, and convenient methods [8]. Wang and Wang [48] highlighted the limited availability of publications specifically addressing the topic of nonuniform beams, where the density and flexural rigidity varied along the longitudinal axis, even when material graduation was not considered. Wu *et al.* [49] studied the semi-inverse method to find solutions for the dynamic equation of inhomogeneous, axially FG, simply supported beams. Li *et al.* [50] also analyzed the free vibration of axially inhomogeneous FG beams. The frequency equations of beams with various end conditions were derived in closed form. One study on nonuniform and axially FG beams is the free vibration of axially functionally nonuniform graded beams, which Huang and Li [15] presented as a new approach. They investigated the free vibration of axially FG beams with nonuniform cross-sections, considering varied bending stiffness and mass density levels. As part of a study that also examined gradient variation using the integral equation method, Alshorbagy *et al.* [51] applied the finite element method to analyze the dynamic characteristics of beams with material graduation axially or transversally through the thickness. Making a valuable contribution to the literature on nonuniform cross-section axially FG beams, Shahba *et al.* [52] presented a finite element method for the structural analysis of axially nonuniform FG Euler–Bernoulli beams. They proposed a new finite element to shape the functions of uniform homogeneous Euler-Bernoulli beams. Moreover, Kukla and Rychlewska [53] proposed a free vibration analysis approach for axially nonuniform FG beams. Their approach replaced functions characterizing FG beams with piecewise exponential functions. Additionally, Cao *et al.* [42] analyzed the free vibration of an axial FG Euler-Bernoulli tapered beam and detailed the analytical equations based on perturbation theory and the Meijer G-function. Mahmoud in [54] used the lumped mass transfer matrix method for free vibration analysis of nonuniform and stepped axial FG beams with any number of point masses. Sharma *et al.* [55] investigated the natural frequencies of an axially tapered clamped-clamped FG beam. The results of the material grading and geometry of the FG beam were obtained using the generalized differential quadrature method. Kondakçıand Coşkun [56] examined the axial vibration of nonuniform and FG rods using an analytical-based numerical approach. The proposed method combined analytical formulations with numerical techniques

to account for the effects of material gradation and geometric nonuniformity on vibration characteristics. Jedrysiak [57] also investigated axially FG beams in a study that theoretically modeled dynamics and stability. The method used employed tolerance modeling – a mathematical framework that accounts for material gradation and structural variations along the beam axis – to analyze its dynamic behavior and stability. Wang *et al.* [58] investigated the dynamics of axially moving beams made of functionally graded materials using the interpolating matrix method. Chun and Zheng [59] developed a three-dimensional solution for FG plates using the Haar wavelet method. They demonstrated how applicable and effective the method was for analyzing the vibration and deformation of FG rectangular plates with arbitrary material gradient distributions. Hein and Feklistova [8] used the 'Haar matrix' as a potential solution. They presented a study on the Haar wavelet method, which was proposed as a simple and fast solution for free vibrations in axially FG beams with different boundary conditions and varying cross-sectional areas. Additionally, Majak *et al.* [60] developed a new high-order Haar wavelet method for solving differential and integrodifferential equations, improving the accuracy and speed of convergence of the solution. Continuing with the Haar wavelet method for FG beam research, Kirs *et al.* [61] presented a study on the free vibration analysis of axially uniform FGM beams, employing the Haar wavelet method and comparing the solutions obtained with those produced via the finite difference and differential quadrature methods. One of the latest works by Kim *et al.* [62] investigated the free vibration analysis of laminated composite shells with varying thicknesses. They used the Haar wavelet discretization method to analyze the shell with a thickness varying along the meridional direction. Recently, Mikola *et al.* [63] investigated the vibration analysis of functionally graded beams using a higher-order Haar wavelet method. Their method extended the traditional Haar wavelet approach to accommodate higher-order accuracy, enabling the precise modeling of material grading and beam dynamics. The Haar wavelet method (HWM) and its higher-order extensions have recently gained prominence as efficient numerical tools for solving complex differential equations in engineering applications. Early contributions by Aziz *et al.* advanced the classical Haar framework through improved formulations for nonlinear integral and integro-differential equations, thereby establishing a foundation for higher-order wavelet schemes [64]. Building upon these developments, Ratas *et al.* demonstrated the versatility of the higher-order Haar wavelet method (HOHWM) in addressing nonlinear boundary value problems and partial differential equations, including adaptive and nonuniform grids that enhanced solution accuracy [65, 66]. Kivistik *et al.* [67] further extended the application of HOHWM to structural dynamics and flight mechanics, highlighting its capability in analyzing transient and dynamic responses of complex systems. In the field of structural mechanics, Mehrparvar *et al.* successfully applied HOHWM to free vibration analyses of Timoshenko beams, including tapered configurations, confirming its computational efficiency and robustness for geometrically nonuniform structures [67, 68]. Likewise, Jena *et al.* [69] employed Haar and higher-order Haar formulations for investigating the dynamic behavior of nanobeams, illustrating the applicability of the method to multi-scale problems. Collectively, these studies show that wavelet-based discretization is not only highly accurate and rapidly convergent but also capable of handling structures exhibiting significant geometric and material complexity. Motivated by these advances, the present work applies the Haar wavelet method to the modal analysis of axially functionally graded Euler-Bernoulli beams with nonuniform cross-sections, particularly tapered and cone-shaped geometries that have not yet been explored in existing literature.

In this study, a numerical approach based on the Haar wavelet method is revisited to investigate the free vibration of FGM beams with variable conditions, such as various beam supports, cross-sections, and material properties. To demonstrate the convergence, efficiency, and accuracy of the Haar wavelet method, some numerical examples are presented for the free vibrations of FGM beams. For validation of this method, the results are compared with examples available in the literature solved using different methods. The effects of some geometrical and material parameters on the natural frequencies are also discussed. This study demonstrates the convenient and efficient application of the Haar wavelet method to analyze the free vibrations of FG beams. We also present extended results for benchmarking purposes. To this end, we extend the application of the Haar wavelet method for EB beams for different materials and cross-sectional variations, the effectiveness of which was previously proven by Hein and Feklistova [8]. These cases have not previously been solved using this method, and in the few available studies, only the first natural vibration frequencies were reported. In this study, the first, second, third, and fourth natural frequencies are presented for each problem, providing results that have not been previously reported in the literature.

The proposed model has broad applicability in modern engineering fields where both material gradation and geometric nonuniformity are present. Functionally graded beams with tapered or variable cross-sections are widely used in aerospace engineering, such as in aircraft wings, turbine blades, and fuselage panels, where weight reduction and vibration resistance are critical. In civil engineering, nonuniform axially graded beams can be found in bridge girders, high-rise structural members, and other infrastructure elements designed to optimize strength-to-weight ratios. Similarly, in mechanical engineering, graded shafts, machine components, and rotating elements often exhibit both axial material variation and nonuniform cross-sections. The ability to accurately predict their dynamic response is essential for ensuring performance, safety, and durability [2, 3, 5, 6, 33]. The present study, therefore, provides a reliable framework for analyzing the free flexural vibration of such advanced structural elements.

2. HAAR WAVELET METHODS

Alfred Haar [70] introduced a novel structure that is confined to a finite interval and lacks continuous differentiability. This innovative concept led to the development of the Haar wavelet, which

is an orthogonal system defined within the interval [0, 1]. Haar wavelets, characterized by their simplicity, are constructed from single rectangular block-pulses, making them one of the most elementary wavelet forms [71]. Saeedi *et al.* [72] pointed out that using wavelet-based techniques to transform integral equations into algebraic equations significantly simplifies the computational process and enhances the efficiency of a solution. Despite their straightforward nature, Haar wavelets possess powerful analytical properties, such as orthogonality and compact support, which make them a useful tool in solving differential equations, data compression, and other computational problems. In this section, we first outline the structure of the Haar wavelets and then introduce the procedure for solving differential equations based on the Haar wavelet method.

2.1. Basics of Haar wavelets

The Haar wavelet family for $x \in [A, B]$, where A and B are as-given constant values, may be defined as follows [16]:

$$h_i(x) = \begin{cases} 1 & x \in [\xi_1(i), \xi_2(i)), \\ -1 & x \in [\xi_2(i), \xi_3(i)), \\ 0 & \text{elsewhere}, \end{cases} \tag{1}$$

where h is the Haar wavelet, and the appearing terms in (1) may be given as

$$\begin{aligned} \xi_1(i) &= A + 2k\mu\Delta x, \\ \xi_2(i) &= A + (2k+1)\mu\Delta x, \\ \xi_3(i) &= A + 2(k+1)\mu\Delta x, \quad \mu = \frac{M}{m}, \end{aligned} \tag{2}$$

where index i in (1) is a wavelet number and is calculated with $i = m + k + 1$. The parameter m corresponds to the resolution and is defined with $m = 2^j$. j is the scale parameter ($j = 0, 1, \ldots, J$), J denotes the maximal level of resolution, M denotes the half-distance of the wavelet spacing, and $M = 2^J$. $2M$ divides the interval $[A, B]$ into subintervals of equal length, using the length of each subinterval defined with $\Delta x = (B - A)/2M$. k is the factor of delay that determines the position of the wavelet in the x-axis, and $k = 0, 1, \ldots, m-1$.

The width of i-th wavelet is defined by

$$\xi_3(i) - \xi_1(i) = 2\mu\Delta x = (B - A)m^{-1} = (B - A)2m^{-1}. \tag{3}$$

In the Haar function, if j increases, the distance between the wavelets decreases. Thus, the resolution and convergence become more pronounced. If k changes from to $m - 1$, the initial point of the i-th wavelet $\xi_1(i)$ moves from $x = A$ to $x = [A + (m - 1)B]/m$. The parameters j and k determine the frequency of the number of subintervals.

The Haar wavelet family consists of orthogonal functions, so the following relation holds:

$$\int_A^B h_i(x)h_l(x)\,\mathrm{d}x = \begin{cases} (B - A)2^{-j}, & l = i, \\ 0, & l \neq i. \end{cases} \tag{4}$$

2.2. Solution of ordinary differential equations

The Haar wavelet is discontinuous at some points due to its structure, and since there are no derivatives at these points, we cannot directly apply the derivatives to the Haar wavelets [73]. Cattani [74] addressed the discontinuity problem by combining piecewise constant Haar functions with spline interpolations. Cattani observed that Haar functions naturally align with discontinuous functions due to their piecewise constant structure. However, a key limitation of piecewise constant Haar functions is their inability to ensure continuous differentiability, which can impact the accuracy and smoothness of solutions in certain problems. Spline interpolations are introduced to address the requirements for continuity and differentiability. By providing smooth transitions in the solution, spline interpolations effectively resolve uncertainties. Cattani integrated these two methods to leverage their respective strengths [74, 75]. Chen and Hsiao [76] assumed that the highest-order derivative is equal to the Haar function and subsequently integrated this Haar function. They presented a method in which the solution is obtained by substituting the boundary conditions of the problem into the resulting set of equations. Lepik and Hein [16] generalized the method for higher-order differential equations and established an algorithm, structuring the solution interval according to the uniform and nonuniform cases in the solutions of differential equations with Haar wavelets. Following the method of Lepik and Hein [16], a higher-order differential equation with the boundaries A, B and initial conditions may be given as

$$\sum_{\nu}^{n} A_\nu(x) y^{(\nu)}(x) = f(x) \quad x \in [A, B], \tag{5}$$

$$y^{(\nu)}(\alpha) = y_0^{(\nu)} \quad (\nu = 0, 1, \ldots, n-1), \tag{6}$$

where $A_\nu(x)$ and $f(x)$ are known functions, $y^{(\nu)}$ is the derivative of the sought function with respect to x, ν is the order of the derivative, n is the highest-order derivative, $y^{(\nu)}(A)$ is the initial condition and $y_0^{(\nu)}$ is the constant value of the initial condition. For the Haar wavelet solution, the highest-order derivative may be taken as

$$y^{(n)}(x) = \sum_{i=1}^{2M} a_i h_i(x_l), \tag{7}$$

where a_i is the wavelet coefficient. By integrating equation (7) $n - \nu$ times, the sought function may be constructed as

$$y^{(\nu)}(x) = \sum_{i=1}^{2M} a_i p_{n-\nu,i}(x) + Z_\nu(x),$$

where

$$Z_\nu(x) = \sum_{\sigma=0}^{n-\nu-1} \frac{1}{\sigma!}(x - A)^\sigma y_0^{(\nu+\sigma)}. \tag{8}$$

The integral of the Haar wavelets may be given as follows [73]:

$$\begin{aligned} p_{\nu,i}(x) &= \int_A^x \int_A^x \cdots \int_A^x h_i(t)\,\mathrm{d}t^{\nu} \\ &= \frac{1}{(\nu-1)!}\int_A^x (x-t)^{\nu-1} h_i(t)\,\mathrm{d}t, \\ &\nu = 1, 2, \ldots, n, \quad i = 1, 2, \ldots, 2M, \end{aligned} \tag{9}$$

where A is the initial value, and t is the derivation variable. Considering equations (1) and (9), the form present after integrating the Haar wavelets may be given as [16]

$$p_{\alpha,i}(x) = \begin{cases} 0, & x < \xi_1(i), \\ \dfrac{1}{\alpha!}\left[x-\xi_1(i)\right]^{\alpha}, & x \in \left[\xi_1(i), \xi_2(i)\right], \\ \dfrac{1}{\alpha!}\left\{\left[x-\xi_1(i)\right]^{\alpha} - 2\left[x-\xi_2(i)\right]^{\alpha}\right\}, & x \in \left[\xi_2(i), \xi_3(i)\right], \\ \dfrac{1}{\alpha!}\left\{\left[x-\xi_1(i)\right]^{\alpha} - 2\left[x-\xi_2(i)\right]^{\alpha} + \left[x-\xi_3(i)\right]^{\alpha}\right\}, & x > \xi_3(i), \end{cases} \tag{10}$$

where α is the order of the integrated Haar wavelet, and $p_{\alpha,i}(x)$ is the integrals of the Haar wavelets in the vector form. These equations are valid for $i > 1$. For $i = 1$, $\xi_1 = A$, and $\xi_2 = \xi_3 = B$ and considering equation (10), $p_{\alpha,1}(x)$ can be given with

$$p_{\alpha,1}(x) = \frac{1}{\alpha!}(x-A)^{\alpha}. \tag{11}$$

For numerical solutions, Haar wavelets should be obtained in discrete form. The collocation method is often used for discretization [16]. If the points calculated are used with fixed intervals (uniform grid), the intervals are obtained as follows:

$$\tilde{x}_l = A + l\Delta x \quad l = 0, 1, \ldots, 2M. \tag{12}$$

Collocation points are defined as the midpoint of the sub-steps and may be given as

$$x_l = 0.5\left(\tilde{x}_{l-1} + \tilde{x}_l\right) \quad l = 1, \ldots, 2M. \tag{13}$$

By replacing x with x_l in (1), (10), and (11), Haar matrices may be obtained when defined at the relevant points. The Haar matrices with $2M \times 2M$ dimensions are defined in the interval $[A, B]$ and indicated with the symbols $\mathbf{H}$, P_1, $\mathbf{P}_2$, …, $\mathbf{P}_{\nu}$. The matrices have the forms of $\mathbf{H}(i,l) = h_i(x_l)$, $\mathbf{P}_{\nu}(i,l) = p_{\alpha,i}(x_l)$ and $(\nu = 0, 1, \ldots)$.

After collocation, we can construct the governing equations as a system of linear algebraic equations. The solution to the equation system gives the unknown a_i terms, which are needed to construct the discretized approximate function in the form of (8).

3. FREE VIBRATION OF ANALYSIS OF NONUNIFORM FG MATERIAL EB BEAMS

L is the beam length, and ξ is the beam axis variable. The governing equation of the free vibration of the Euler-Bernoulli beam with variable density, modulus of elasticity, and cross-section can be represented via the following formula after nondimensionalization with $x = \xi/L$ [8]:

$$\frac{d^2}{dx^2}\left[E(x)I(x)\frac{d^2y(x)}{dx^2}\right] - k^4 m(x)y(x) = 0, \quad x \in [0, 1], \tag{14}$$

where x is a dimensionless beam axis variable, $y(x)$ is the vertical displacement, $m(x) = \rho(x)A(x)$ is the mass, $\rho(x)$ is the density of the beam material, $E(x)$ is the modulus of elasticity, $A(x)$ is the beam cross-sectional area and $I(x)$ is the cross-sectional moment of inertia. $k^4 = \dfrac{\rho_0 A_0 \omega^2 L^4}{E_0 I_0}$ is the coefficient that determines the natural vibration frequencies, where k is the natural frequency, while ρ_0, A_0, E_0 and I_0 are the density of the beam, the cross-sectional area, the modulus of elasticity, and the moment of inertia, respectively, at the beam initial point. Following Hein and Feklistova [77], after evaluating the derivatives, the governing equation for the vibration may be given as

$$\begin{aligned} &\frac{d^4y(x)}{dx^4}E(x)I(x) + 2\frac{d^3y(x)}{dx^3}\left[\frac{dE(x)}{dx}I(x) + \frac{dI(x)}{dx}E(x)\right] \\ &\quad + \frac{d^2y(x)}{dx^2}\left[\frac{d^2E(x)}{dx^2}I(x) + 2\frac{dE(x)}{dx}\frac{dI(x)}{dx}\right. \\ &\quad \left. + \frac{d^2I(x)}{dx^2}E(x)\right] - k^4 y(x)\rho(x)A(x) \\ &\quad = 0, \quad x \in [0, 1]. \end{aligned} \tag{15}$$

Here, d/dx is the derivation operator with respect to x. Equation (15) gives the free vibration of an EB beam in the most general case, and it is extremely complex to solve. An analytical solution for the general case of (15) is not possible in many cases, so a numerical solution can be obtained using the Haar wavelet method. Following the procedure in Section 2.2, we can evaluate the derivatives in order:

$$\begin{aligned} y'^{\nu}(x) &= \sum_{i=1}^{2M} a_i h_i(x), \\ y'''(x) &= \sum_{i=1}^{2M} a_i p_{1,i}(x) + y'''(0), \\ y''(x) &= \sum_{i=1}^{2M} a_i p_{2,i}(x) + y'''(0)x + y''(0), \\ y'(x) &= \sum_{i=1}^{2M} a_i p_{3,i}(x) + \frac{1}{2}y'''(0)x^2 + y''(0)x + y'(0), \\ y(x) &= \sum_{i=1}^{2M} a_i p_{4,i}(x) + \frac{1}{6}y'''(0)x^3 + \frac{1}{2}y''(0)x^2 \\ &\quad + y'(0)x + y(0). \end{aligned} \tag{16}$$

By following the procedure outlined in Section 2.2, derivatives can be systematically evaluated in sequence. For an n-th order linear ordinary differential equation, the term involving the highest-order derivative is represented using Haar functions, as shown in (7). Through the application of (7) and (8), the integrals of Haar wavelets necessary for solving differential equations are derived.

To solve the Euler-Bernoulli beam equation and determine $y(x)$, which represents vertical displacement, it is crucial to compute the integrals of the highest-order Haar functions. These integrals, represented as $p_{\alpha i}(x)$ in (10), are expressed in the vector form of Haar wavelets. The initial conditions for this differential equation are defined in (6) as $y^{(\nu)}(\alpha) = y_0^{(\nu)}$. Using these initial conditions, the explicit expression for $y(x)$ is formulated, as presented in (16).

Substituting $y(x)$ and its derivatives into (15) and incorporating the relevant support conditions allows for solving the equation of motion. In essence, the solution is achieved by substituting the boundary condition values into the Haar functions based on the beam support configuration.

In this study, four distinct support cases were analyzed to demonstrate the applicability of the method under various boundary conditions:

- For the clamped-free (C-F) supported beam, it is clamped at $x = 0$ and free at $x = 1$. The boundary conditions are defined as $y(0) = y'(0) = 0$, $y''(1) = y'''(1) = 0$. By substituting the boundary conditions in appropriate terms of (16), we can obtain the unknown initial conditions from

$$\begin{aligned} \sum_{i=1}^{2M} a_i p_{1,i}(1) + y'''(0) &= 0, \\ \sum_{i=1}^{2M} a_i p_{2,i}(1) + y'''(0) + y''(0) &= 0. \end{aligned} \tag{17}$$

- For a simply supported beam (P-P), the boundary conditions at the supports are defined as $y(0) = y''(0) = 0$, $y(1) = y''(1) = 0$. Using (16), the system of linear equations that gives the unknown initial conditions is given as

$$\begin{aligned} \sum_{i=1}^{2M} a_i p_{2,i}(1) + y'''(0) &= 0, \\ \sum_{i=1}^{2M} a_i p_{4,i}(1) + \frac{1}{6} y'''(0) + y'(0) &= 0. \end{aligned} \tag{18}$$

- The boundary conditions for a beam (C-C) clamped at both ends are $y(0) = y'(0) = 0$, $y(1) = y'(1) = 0$. One may obtain initial conditions employing (16) as

$$\begin{aligned} y'''(0) &= 6 \sum_{i=1}^{2M} a_i \left(2p_{4,i}(1) - p_{3,i}(1)\right), \\ y''(0) &= \sum_{i=1}^{2M} a_i \left(2p_{3,i}(1) - 6p_{4,i}(1)\right). \end{aligned} \tag{19}$$

- For a beam clamped at one end $x = 0$ and simply supported at the other $x = 1$ (C-P), the boundary conditions are $y(0) = y'(0) = 0$, $y(1) = y''(1) = 0$. Analogically, (16) derives initial conditions for this case as

$$\begin{aligned} y'''(0) &= \sum_{i=1}^{2M} a_i \left(3p_{4,i}(1) - \frac{3}{2} p_{2,i}(1)\right), \\ y''(0) &= \sum_{i=1}^{2M} a_i \left(-\left(3p_{4,i}(1) - \frac{3}{2} p_{2,i}(1)\right) - p_{2,i}(1)\right). \end{aligned} \tag{20}$$

Equation (15), which expresses axially nonuniform FG EB beam vibration, can be solved by substituting the boundary conditions derived from the support conditions. For this procedure, we must discretize the final form of (15). The discretized system is a system of linear algebraic equations obtained by replacing x with x_l in (15). Unlike the classical method [16], we evaluated the Jacobian of the discrete governing equation with respect to a_i, obtaining the characteristic frequency matrix that gives natural frequencies. After evaluating the determinant of the frequency matrix, the characteristic n-th order polynomial equation can be determined and solved for the angular natural frequencies from lowest to highest. Subsequent to the determination of the frequencies, we can easily obtain the mode shapes for solving the linear system of equations for the corresponding frequency. In this case, the frequency k should be substituted into the equations, and the system of linear equations should be solved for a_i values. By taking $\nu = 0$ and substituting the discrete form a_i values into (8), the mode shapes may be obtained.

4. RESULTS AND DISCUSSION

This section presents a comparative study of FG beam examples solved using various methods taken from the literature, with the Haar wavelet solutions of this work. We first present beams with a uniform cross-sectional area and no material variation. The dimensionless natural frequencies (DNFs) were calculated using the Haar wavelet method under different boundary conditions along the x-axis of the cross-section. The subsequent comparisons focus on beams with nonuniform cross-sections but no material variation, analyzing their DNFs under various boundary conditions using the Haar wavelet method. Finally, the DNF results for beams with simultaneous variations in both cross-section and material properties are presented in detail. All calculations presented in this work were performed using the Haar wavelet method coded with MATLAB [78]. The Haar wavelet matrices and functions were constructed as described in Section 2, and the steps outlined in Section 3 were applied to conduct the analysis.

In the Haar wavelet method, the resolution parameter J is a key factor that influences the accuracy of the solution. In this study, to realize precision analyses, DNF calculations are performed for $J = 3, 4$, and 5, and comparisons are made with values reported in previous studies for the resolution level of 5. $J = 5$ is sufficient for dimensionless natural frequency calculation, and the resolution

value of $J = 5$ was used for the remaining calculations. Figure 1 illustrates the modal shape of the first frequency for the clamped beam at different resolutions. As shown in Fig. 1, values closer to 1 are calculated at $J = 5$. The curve becomes smoother as the resolution level increases.

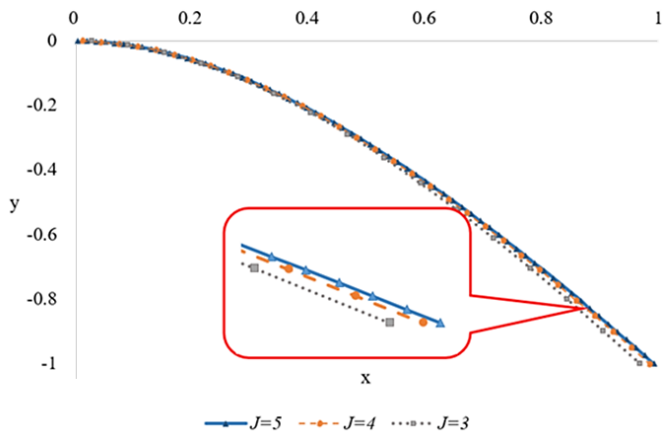

Fig. 1. The variation in the first frequency mode shape of the C-F beam with different J levels

The computations were performed on a laptop equipped with an Intel(R) Core (TM) i7-10875H CPU 2.30 GHz, 32.0 GB RAM, and a 64-bit operating system, ensuring efficient execution of the numerical procedures. For the highest level of resolution ($J = 5$), the highest time consumption was about six minutes across all the cases.

There are no known restrictions on the application of this method, and it can be used to solve highly complex problems [16]. However, as is typical for numerical methods, increasing the resolution leads to larger matrix dimensions and, consequently, higher time consumption. While this may act as a limiting factor, it is observed that even at a relatively high resolution, such as $J = 5$, the time consumption remains remarkably low.

4.1. Uniform cross-section, various materials in FG beams

In a homogeneous beam with a uniform cross-sectional area, no material variation occurs. The governing equation for beam vibrations is (14). Hence, $D = EI$ and $m = \rho A$ are considered constants. For the uniform cross-section type, a beam of FG material inhomogeneous in the axial direction, the material model is given as an exponential function as follows [15]:

$$Q(x) = \begin{cases} Q_0\left(1 - \dfrac{e^{\beta x} - 1}{e^{\beta} - 1}\right) + Q_1 \dfrac{e^{\beta} - 1}{e^{\beta} - 1}, & \beta \neq 0, \\ Q_0(1 - x) + Q_1 x, & \beta = 0. \end{cases} \tag{21}$$

In equation (21), the parameters Q_0 and Q_1 are the material properties at the ends $x = 0$ and $x = 1$, respectively, such as ρ_0, ρ_1, E_0 and E_1. Here, β is the gradient parameter describing the volume fraction distribution of the material in the FG beam cross-section.

In this study, the materials chosen are aluminum and zirconium, and their properties are shown in (22):

$$\begin{aligned} \text{Al}: &\quad E_0 = 70\ \text{GPa}, &\quad \rho_0 = 2702\ \frac{\text{kg}}{\text{m}^3}, \\ \text{ZrO}_2: &\quad E_1 = 200\ \text{GPa}, &\quad \rho_1 = 5700\ \frac{\text{kg}}{\text{m}^3}. \end{aligned} \tag{22}$$

Here, for axial nonhomogeneity, the material properties at each end were aluminum and zirconium, respectively, measured using gradient parameters. In Fig. 2, the axially FG beam with a uniform cross-sectional area and variable modulus of elasticity is illustrated. By selecting different gradient parameter values (β), the distribution of the modulus of elasticity for the constituent materials – aluminum and zirconium – along the beam axis is represented. Likewise, (21) is valid for the density, and the same gradient view appears depicted in Fig. 2.

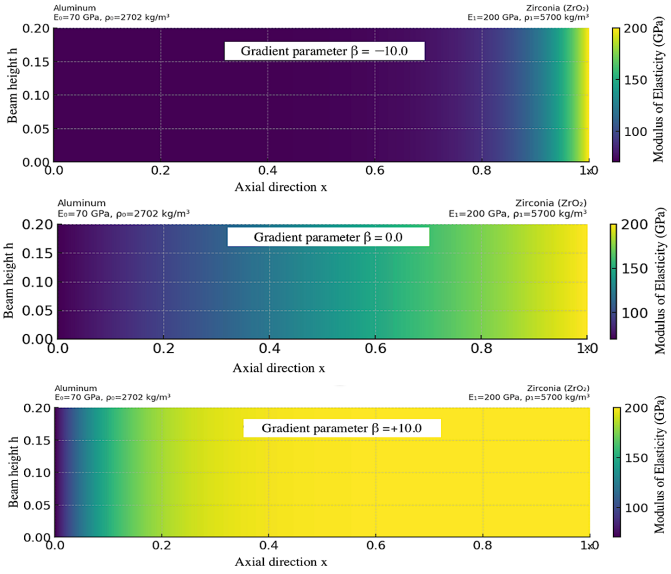

Fig. 2. The distribution of the modulus of elasticity for the gradient parameter β in an axially FG beam

In their study, Huang and Li [15] adopted aluminum and zirconium as the two constituent materials, corresponding to a stiffness ratio of $Q_1/Q_0 = 3$. This exponential model, illustrated in Fig. 3, effectively captures the influence of the gradient parameter on the variation of material properties along the beam length and has since been widely adopted in subsequent axially FG beam vibration analyses.

In Tables 1–4, the dimensionless natural frequencies with various support conditions are shown for the uniform cross-section with axial nonhomogeneity. The first frequencies of the homogeneous beam are presented in the last rows of Tables 1–4. Moreover, the tables show that the available frequency value is compared with the corresponding value of this work, and the results are validated. After the result validation, the other frequency values are given to highlight new contributions of this study to the literature.

In Table 1, the dimensionless natural frequencies are calculated for a uniform C-F beam with axial nonhomogeneity. We

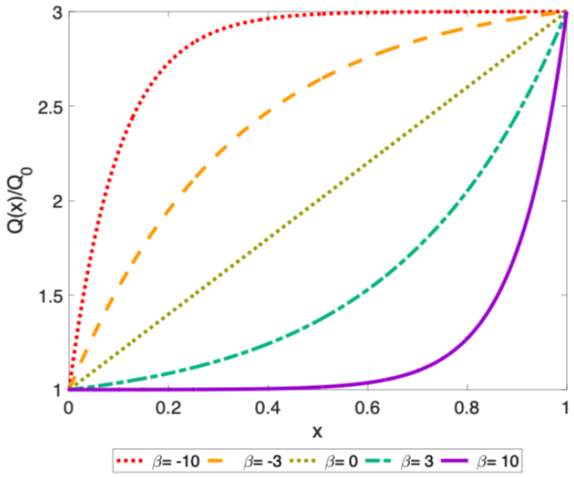

Fig. 3. The variation of the material properties for the gradient parameter β with $Q_1/Q_0 = 3$. Various materials (21)

observe that as the resolution value increases, the results match those of Huang and Li [15]. The maximum deviation occurs at $\beta = -10$; however, in other cases, the dimensionless natural frequencies are in excellent agreement.

Table 1
The first four DNFs for FGM C-F beam uniform cross-sections

n	β	Present $J=3$	Present $J=4$	Present $J=5$	[15]	Dev. (%) from [15]
1	−10	3.4168	3.5091	3.5269	3.5656	1.0840
2		23.2093	23.5974	23.6734	–	–
3		67.2793	67.9583	68.0871	–	–
4		134.7844	135.2301	135.2934	–	–
1	−3	3.1242	3.1370	3.1399	3.1421	0.0694
2		23.0342	23.0491	23.0513	–	–
3		67.7624	67.5512	67.4948	–	–
4		135.6123	134.5209	134.2458	–	–
1	0	2.9218	2.9247	2.9254	2.9256	0.0076
2		22.4073	22.3672	22.3572	–	–
3		66.6350	66.2847	66.1980	–	–
4		133.1987	131.8624	131.5343	–	–
1	3	2.8484	2.8529	2.8541	2.8544	0.0112
2		21.5439	21.5071	21.4979	–	–
3		64.1147	63.7813	63.6989	–	–
4		128.2698	126.9940	126.6810	–	–
1	10	3.0059	3.0339	3.0408	3.0431	0.0762
2		20.6677	20.7185	20.7315	–	–
3		60.3560	60.2239	60.1932	–	–
4		121.1880	120.2867	120.0707	–	–
Homogeneous beam				3.5162	3.516	0.0056

In Table 2, we show the values of dimensionless natural frequencies for a uniform simply supported beam (P–P) according to variations in the material property gradient parameter β. We compare our results with those of Huang and Li [15] and Hein and Feklistova [8]. The largest deviation from Huang and Li [15] is for $\beta = -10$. When comparing our results with the frequencies of Hein and Feklistova [8], we achieve excellent agreement; thus, we confirm the accuracy of our study and the reliability of its higher-order natural frequencies.

Table 2
The first four DNFs for FGM P-P beam uniform cross-sections

n	β	Present $J=3$	Present $J=4$	Present $J=5$	[15]	[8]	Dev. (%) from [15]	Dev. (%) from [8]
1	−10	11.3687	11.4270	11.4481	11.4532	11.4481	0.0446	0.0000
2		45.4617	45.6004	45.6628	–	–	–	–
3		102.5854	102.5572	102.6170	–	–	–	–
4		183.3468	182.4625	182.3706	–	–	–	–
1	−3	11.2129	11.2361	11.2422	11.2443	11.2422	0.0186	0.0000
2		44.8405	44.8487	44.8523	–	–	–	–
3		101.1946	100.9026	100.8340	–	–	–	–
4		180.8165	179.5244	179.2122	–	–	–	–
1	0	10.8611	10.8650	10.8660	10.8663	10.866	0.0027	0.0001
2		43.7483	43.6848	43.6691	–	–	–	–
3		98.7052	98.2637	98.1542	–	–	–	–
4		176.3480	174.8145	174.4349	–	–	–	–
1	3	10.3688	10.3673	10.3670	10.3669	10.367	0.0007	0.0002
2		42.0768	41.9951	41.9749	–	–	–	–
3		95.1313	94.6595	94.5426	–	–	–	–
4		170.0761	168.5137	168.1276	–	–	–	–
1	10	9.9369	9.9365	9.9366	9.9358	9.9366	0.0077	0.0003
2		40.1538	40.0890	40.0738	–	–	–	–
3		91.0758	90.6586	90.5577	–	–	–	–
4		163.1480	161.7094	161.3596	–	–	–	–
Homogeneous beam				9.8701	9.8696	–	0.0051	–

Table 3 demonstrates the dimensionless natural frequencies for a uniform inhomogeneous C-P beam. The greatest deviation from Huang and Li [15] is found for the value of $\beta = -10$. The other β cases have good matches as dimensionless natural frequencies.

Table 4 presents the dimensionless natural frequencies for a uniform FGM C-C beam. The results of this study are in close agreement with the first natural frequency values reported in the literature. The largest deviation rate occurs for $\beta = -10$, where the first frequency presented by Huang and Li [15] has a deviation of 0.01277%.

In the studies presented so far, only the first natural frequencies have been reported. The frequencies calculated by the Haar wavelet method in this study have great agreement with the first frequencies given in the references. According to the estimated additional frequencies in this work, generally, all frequencies tend to decrease in all support cases while β increases. However, this statement is untrue in some cases, such as C-C and C-F: The first frequency of the C-F beam accepts the general tendency of $\beta = 10$. At $\beta = 10$, the first frequency exhibits an increase in value. The first frequency of the C-C beam increases from $\beta = 0$ and again decreases at $\beta = 10$.

Table 3
The first four DNFs for FGM C-P beam uniform cross-sections

n	β	Present $J=3$	Present $J=4$	Present $J=5$	[15]	[8]	Dev. (%) from [15]	Dev. (%) from [8]
1	−10	15.9939	16.3185	16.3837	16.4775	16.3837	0.5694	0.0001
2		53.8972	54.6866	54.8484	–	–	–	–
3		114.9901	116.0680	116.2897	–	–	–	–
4		199.9095	200.5959	200.7299	–	–	–	–
1	−3	15.9627	16.0109	16.0219	16.0307	16.0307	0.0549	0.0549
2		54.4139	54.4578	54.4654	–	–	–	–
3		115.9050	115.6207	115.5438	–	–	–	–
4		200.9101	199.5248	199.1739	–	–	–	–
1	0	15.8659	15.8715	15.8729	15.8734	15.8729	0.0030	0.0002
2		54.0732	53.9872	53.9657	–	–	–	–
3		114.4905	113.9491	113.8148	–	–	–	–
4		197.7408	195.9455	195.5028	–	–	–	–
1	3	15.7207	15.7178	15.7171	15.7171	15.7171	0.0000	0.0000
2		52.9510	52.8390	52.8112	–	–	–	–
3		111.3820	110.7980	110.6534	–	–	–	–
4		191.8021	189.9642	189.5110	–	–	–	–
1	10	15.4956	15.4954	15.4956	15.493	15.493	0.0169	0.0169
2		50.9128	50.8218	50.8003	–	–	–	–
3		106.9954	106.4728	106.3464	–	–	–	–
4		184.3359	182.6329	182.2194	–	–	–	–
Homogeneous beam				15.4191	15.4182	–	0.0059	–

Table 4
The first four DNFs for FGM C-C beam uniform cross-sections

n	β	Present $J=3$	Present $J=4$	Present $J=5$	[15]	[8]	Dev. (%) from [15]	Dev. (%) from [8]
1	−10	23.4880	23.9360	24.0269	24.0576	24.0269	0.1277	0.0000
2		66.9180	67.8430	68.0347	–	–	–	–
3		133.8400	135.0000	135.2376	–	–	–	–
4		224.7100	225.3000	225.4194	–	–	–	–
1	−3	23.8570	23.9230	23.9384	23.9456	23.9384	0.0301	0.0000
2		67.7110	67.7490	67.7540	–	–	–	–
3		134.9500	134.5700	134.4732	–	–	–	–
4		225.8000	224.1400	223.7196	–	–	–	–
1	0	24.3670	24.3730	24.3749	24.3752	24.3749	0.0014	0.0002
2		67.7510	67.6280	67.5977	–	–	–	–
3		133.7400	133.0600	132.8949	–	–	–	–
4		222.6700	220.5500	220.0284	–	–	–	–
1	3	24.9480	24.9390	24.9371	24.9375	24.9371	0.0016	0.0000
2		67.3170	67.1570	67.1173	–	–	–	–
3		131.2000	130.4700	130.2889	–	–	–	–
4		217.1600	214.9800	214.4412	–	–	–	–
1	10	24.8340	24.8130	24.8080	24.7949	24.808	0.0529	0.0001
2		66.4600	66.2910	66.2487	–	–	–	–
3		128.6000	127.8900	127.7104	–	–	–	–
4		211.7300	209.6600	209.1473	–	–	–	–
Homogeneous beam				22.3750	22.3733	–	0.0076	–

Table 5 displays another validation conducted with different gradient rules. The first three frequencies are compared with those of Huang and Li [15], and the fourth frequency is listed in Table 5 as a new entry in the literature. The material variation can be expressed using trigonometric functions as follows:

$$E(x) = E_0\left[1+\gamma\cos(\pi x)\right],$$
$$\rho(x) = \rho_0\left[1+\delta\cos(\pi x)\right]. \tag{23}$$

In equation (23), the modulus of elasticity and mass density are expressed using parameters $|\gamma|<1$ and $|\delta|<1$, used to describe the variations. Huang and Li [15] used the example from Calio and Elishakoff's study [79] for the P-P beam and expanded their work to other support cases. Calio and Elishakoff [79] demonstrated the closed-form inequality solution for a simply supported beam on an elastic foundation with variable flexural rigidity and mass density for which the axial gradient coefficient $\delta=4\gamma$. According to Calio and Elishakoff [79], for a simply supported beam with $\delta=4\gamma$, the first frequency values remain constant.

Figure 4 illustrates the variation of the modulus of elasticity $E(x)$ along the beam axis for different combinations of the gradient parameters γ. Similar curves can be derived for density using the parameter δ. The curves corresponding to $\delta=4\gamma$ exhibit a wider distribution range and higher $E(x)$ values compared to those obtained for $\delta=\gamma$. In this case, the material stiffness varies more sharply along the beam length, and the contrast between the constituent materials becomes more pronounced. Consequently, the natural frequencies obtained for all boundary conditions are higher and more widely distributed when $\delta=4\gamma$ is used. This behavior indicates that the sensitivity of the dimensionless natural frequency changes significantly with the gradient coefficient δ, which is determined by the selection of the material property parameter γ. Hence, the figure clearly demonstrates the influence of the interaction between γ and δ on the stiffness distribution and dynamic response of the beam. To validate the results of this study, Table 5 is generated

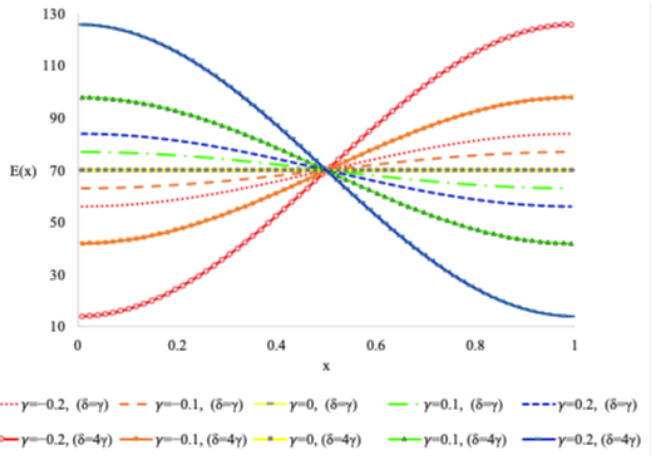

Fig. 4. The variation of the modulus of elasticity for the gradient parameter for $\gamma=\delta$ and $\gamma=\delta/4$. Various materials (23)

Table 5
The first four DNFs for uniform beams with $E(x)$ and $\rho(x)$ and $\delta = 4\gamma$ and $\delta = \gamma$

			$\delta = 4\gamma$					$\delta = \gamma$				
			γ					γ				
	n		−0.2	−0.1	0	0.1	0.2	−0.2	−0.1	0	0.1	0.2
C-F	1	Present	2.5691	2.9716	3.5162	4.3430	5.8909	3.0225	3.2634	3.5162	3.7854	4.0765
		[15]	2.5690	2.9714	3.5160	4.3428	5.8908	3.0224	3.2632	3.5160	3.7853	4.0763
		Dev. (%)	0.0056	0.0070	0.0056	0.0045	0.0024	0.0049	0.0063	0.0056	0.0035	0.0047
	2	Present	20.5526	21.1936	22.0403	23.4127	27.0624	21.2128	21.6311	22.0403	22.4503	22.8728
		[15]	20.5462	21.1877	22.0345	23.4080	27.0597	21.2069	21.6255	22.0345	22.4447	22.8668
		Dev. (%)	0.0320	0.0281	0.0262	0.0201	0.0101	0.0276	0.0260	0.0262	0.0250	0.0263
	3	Present	64.0790	62.0349	61.7313	63.5049	69.9186	61.2580	61.4900	61.7313	61.9929	62.2863
		[15]	64.1287	62.0246	61.7151	63.5303	70.1756	61.2666	61.4838	61.7151	61.9758	62.2737
		Dev. (%)	0.0774	0.0166	0.0263	0.0399	0.3663	0.0141	0.0102	0.0263	0.0275	0.0202
	4	Present	129.0158	122.5591	121.0170	123.6544	134.2614	120.6912	120.8474	121.0170	121.2093	121.4354
P-P	1	Present	9.8701	9.8701	9.8701	9.8701	9.8701	9.8399	9.8626	9.8701	9.8626	9.8399
		[15]	9.8696	9.8696	9.8696	9.8696	9.8696	9.8395	9.8622	9.8696	9.8622	9.8395
		Dev. (%)	0.0051	0.0051	0.0051	0.0051	0.0051	0.0042	0.0045	0.0051	0.0045	0.0042
	2	Present	42.5472	40.2051	39.4863	40.2051	42.5472	39.5282	39.4970	39.4863	39.4969	39.5282
		[15]	42.5405	40.1979	39.4791	40.1979	42.5522	39.5239	39.4905	39.4791	39.4905	39.5239
		Dev. (%)	0.0158	0.0178	0.0184	0.0178	0.0117	0.0110	0.0161	0.0184	0.0161	0.0110
	3	Present	96.7948	90.4663	88.8666	90.4663	96.7948	88.9135	88.8781	88.8666	88.8781	88.9135
		[15]	98.9439	90.4469	88.8481	90.3370	98.6659	90.2491	90.3149	88.8481	90.3149	90.2491
		Dev. (%)	2.1721	0.0214	0.0208	0.1431	1.8964	1.4799	1.5909	0.0208	1.5909	1.4799
	4	Present	172.4599	160.8256	158.0406	160.8256	172.4599	158.0883	158.0523	158.0406	158.0523	158.0883
C-P	1	Present	14.2126	14.7860	15.4191	16.1243	16.9114	14.9205	15.1808	15.4191	15.6376	15.8373
		[15]	14.2117	14.7850	15.4182	16.1235	16.9107	14.9196	15.1799	15.4182	15.6367	15.8365
		Dev. (%)	0.0065	0.0066	0.0059	0.0052	0.0043	0.0057	0.0058	0.0059	0.0059	0.0052
	1	Present	51.5260	50.2045	49.9758	51.1544	54.4758	49.6828	49.8346	49.9758	50.1134	50.2532
		[15]	51.5819	50.2210	49.9742	51.1459	54.4812	49.6719	49.8265	49.9742	50.1206	50.2691
		Dev. (%)	0.1083	0.0329	0.0031	0.0166	0.0098	0.0219	0.0163	0.0031	0.0144	0.0315
	3	Present	110.9079	105.6446	104.2976	106.3442	113.9641	104.1055	104.2023	104.2976	104.3970	104.5059
		[15]	112.9319	108.2707	107.4485	110.4157	119.2732	107.5159	107.5357	107.4485	107.2753	107.0311
		Dev. (%)	1.7922	2.4255	2.9325	3.6874	4.4512	3.1720	3.0999	2.9325	2.6831	2.3593
	4	Present	192.0038	181.1470	178.4194	181.6898	194.9156	178.2828	178.3490	178.4194	178.4982	178.5903
C-C	1	Present	22.3710	22.3738	22.3747	22.3738	22.3710	22.3000	22.3563	22.3747	22.3563	22.3000
		[15]	22.3700	22.3726	22.3735	22.3726	22.3700	22.2984	22.3549	22.3735	22.3549	22.2984
		Dev. (%)	0.0045	0.0052	0.0053	0.0052	0.0045	0.0072	0.0061	0.0053	0.0061	0.0072
	2	Present	64.6623	62.4128	61.6873	62.4128	64.6623	61.6374	61.6752	61.6873	61.6752	61.6374
		[15]	64.7658	62.4327	61.6883	62.4330	64.7668	61.6542	61.6804	61.6883	61.6804	61.6542
		Dev. (%)	0.1598	0.0318	0.0017	0.0323	0.1614	0.0272	0.0084	0.0017	0.0084	0.0272
	3	Present	129.3991	122.7990	120.9642	122.7990	129.3991	120.9389	120.9581	120.9642	120.9581	120.9389
		[15]	138.6441	131.3240	129.2174	131.2343	137.5759	128.7765	129.1098	129.2174	129.1098	128.7780
		Dev. (%)	6.6681	6.4916	6.3870	6.4277	5.9435	6.0862	6.3137	6.3870	6.3137	6.0873
	4	Present	215.8326	203.2821	200.0340	203.2821	215.8326	200.0240	200.0316	200.0340	200.0316	200.0240

for different support conditions, using varying material property values. While the first three dimensionless natural frequencies are presented for comparison, the estimated value of this work, i.e., the fourth frequency, is listed in the last line of each case.

In Table 5, two analyses are listed for different gradient values of δ. Table 5 shows minimal deviation when compared to the results of Huang and Li [15]. In all beam support cases, the frequency values for $\delta = 4\gamma$ exhibit higher values compared to those for $\delta = \gamma$. The significance of this table is that it demonstrates how the sensitivity level of the dimensionless natural frequency varies with the gradient coefficient δ, which is influenced by the selection of the material property parameter γ. Although the Haar wavelet method used in this study exhibits a slight deviation in the third dimensionless natural frequency for P-P and C-C beams, the frequency values for other cases greatly agree with the results of Huang and Li [15], affirming the accuracy of the analysis. Moreover, the calculated first frequency of the P-P beam with $\delta = 4\gamma$ is quite close to π^2 and independent from material variation. This finding is identical to those of Calio and Elishakoff [79] and Huang and Li [15].

4.2. Nonuniform cross-section homogeneous material in FG beams

This section validates the C-F beam and estimates the new dimensionless natural frequency for the remaining cases. The nonuniform cross-section definition of the beam is expressed in terms of beam height $h(x)$ and beam width $b(x)$ as follows:

$$\begin{aligned} h(x) &= h_0\left[1+(\alpha_h-1)x\right], \\ b(x) &= b_0\left[1+(\alpha_b-1)x\right]. \end{aligned} \tag{24}$$

In equation (24), α_h is the ratio of the beam height between its start and end points; similarly, α_b is the ratio in terms of width. A uniform beam should be ($\alpha_b = 1$, $\alpha_h = 1$). Figure 5 illustrates the types of nonuniform beams considered in this study.

Tables 6 and 7 present the first four dimensionless natural frequencies for beams with variable cross-sections made of homogeneous material and different support conditions. Tables 6 and 7 tabulate the frequency characteristics for wedge and cone beams, respectively. Validation for the C-F beam using results

Table 6
The first four DNFs for a nonuniform cross-section with a homogeneous material wedge beam for various supports

n	α	C-F					P-P	C-P	C-C
		[14]	[80]	Present	Dev. (%) from [14]	Dev. (%) from [80]	Present	Present	Present
1	0.1	4.6307	4.63074	4.6305	0.0045	0.0054	3.8697	8.5970	9.8187
2		14.9308	14.9308	14.9248	0.0399	0.0399	18.0380	24.0907	26.8320
3		32.8331	32.83313	32.8118	0.0649	0.0650	39.8123	47.8624	52.3790
4		–	–	58.8916	–	–	69.9001	80.0191	86.4300
1	0.4	3.9343	3.93428	3.9343	0.0006	0.0001	6.4637	11.5520	14.9546
2		17.4879	17.48786	17.4908	0.0167	0.0169	26.5923	34.6801	41.1537
3		44.0248	44.02481	44.0468	0.0501	0.0501	59.5942	70.9306	80.6340
4		–	–	83.6355	–	–	105.7210	120.3326	133.2924
1	0.6	3.7371	3.73708	3.7373	0.0045	0.0050	7.7287	12.9893	17.6339
2		19.1138	19.11381	19.1190	0.0270	0.0269	31.1954	40.2135	48.5878
3		50.3559	50.35366	50.3836	0.0551	0.0595	70.1104	83.0024	95.2527
4		–	–	97.0957	–	–	124.5861	141.3654	157.4976
1	0.7	3.6667	3.66675	3.6670	0.0078	0.0064	8.3017	13.6399	18.8789
2		19.8806	19.88061	19.8863	0.0286	0.0285	33.3567	42.7810	52.0341
3		–	53.3222	53.3543	–	0.0602	75.0204	88.6037	102.0222
4		–	–	103.3731	–	–	133.3648	151.1166	168.7008
1	0.9	–	3.5587	3.5589	–	0.0065	9.3679	14.8497	21.2422
2		–	21.3381	21.3441	–	0.0279	37.4916	47.6472	58.5634
3		–	58.9799	59.0140	–	0.0578	84.3723	99.2187	114.8373
4		–	–	115.3006	–	–	150.0428	169.5862	189.9012
Uniform beam									
1	1	3.516	3.51601	3.5162	0.0056	0.0053	9.8701	15.4191	22.3747
2		22.0345	22.03439	22.0403	0.0262	0.0267	39.4863	49.9758	61.6873
3		61.6972	61.69644	61.7313	0.0553	0.0566	88.8666	104.2976	120.9642
4		–	–	121.0170	–	–	158.0406	178.4194	200.0340

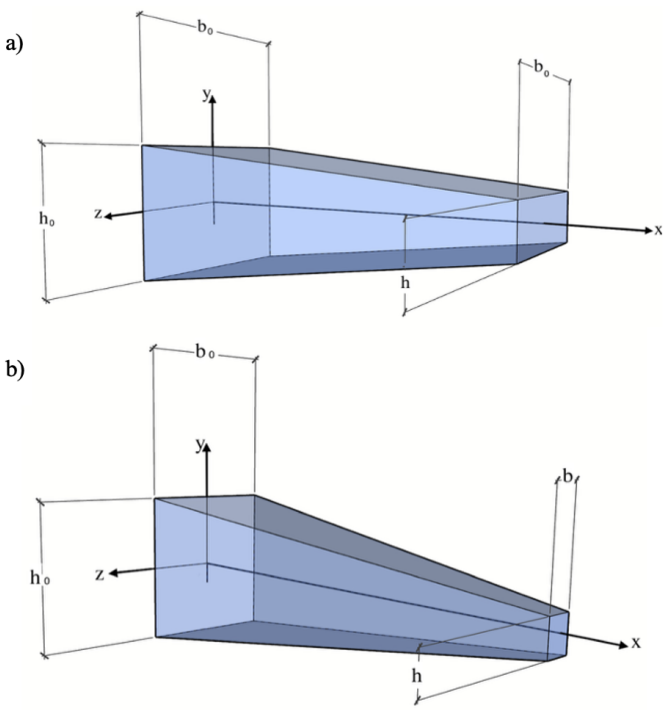

Fig. 5. Nonuniform beams: a) Taper beam, b) Cone beam

from Naguleswaran [14] and Hsu *et al.* [80], as well as results for other support conditions, is provided. To the best of the authors' knowledge, frequencies have not been presented before for all possible support cases except the C-F beam. As seen in Tables 6 and 7, the estimated frequencies of this study exhibit excellent agreement with those in the literature.

Table 6 shows that the first dimensionless natural frequency decreases while the other frequencies increase as the height ratio α increases for the C-F wedge beam ($\alpha_b = 1$, $\alpha_h = \alpha$) [80]. The obtained values are very close to those reported by Naguleswaran [14] and Hsu et al. [80]. The largest deviation in the frequencies rises at $\alpha = 0.1$, and the tapering has the greatest deviation. We observe that for P-P, C-P, and C-C wedge beams, the first four natural frequencies increase with the growth of beam height.

Table 7 presents the dimensionless natural frequencies of cone beams ($\alpha_b = \alpha_h = \alpha$) [80]. Table 7 shows that analogous to the wedge beam configuration, for cone beams with C-F support, the first natural frequency decreases as the beam height, denoted by α, increases, whereas the subsequent frequencies exhibit a trend of increase. The first four P-P, C-P, and C-C beam natural frequencies increase with the growth of the beam height α.

When comparing C-F wedge and cone beams in Tables 6 and 7, we observe that the frequency values of the cone beams

Table 7

The first four DNFs for a nonuniform cross-section with a homogeneous material cone beam for various supports

n	α	C-F					P-P	C-P	C-C
		[14]	[80]	Present	Dev. (%) from [14]	Dev. (%) from [80]	Present	Present	Present
1	0.1	7.2049	7.205	7.2055	0.0082	0.0068	3.0322	9.8737	10.6737
2		18.6802	18.68028	18.6763	0.0209	0.0214	18.9905	25.9597	27.9683
3		37.1238	37.12396	37.0829	0.1103	0.1107	41.2100	50.0329	53.5673
4		–	–	63.3986	–	–	71.5030	82.3241	87.5624
1	0.4	5.009	5.00906	5.0088	0.0035	0.0047	6.2040	12.2256	15.1780
2		19.0649	19.06488	19.0651	0.0011	0.0012	26.8359	35.5396	41.4508
3		45.7384	45.73839	45.7506	0.0267	0.0267	59.9693	71.8716	80.9490
4		–	–	85.4042	–	–	106.1555	121.3095	133.6071
1	0.6	4.3188	4.31879	4.3189	0.0016	0.0019	7.6299	13.4217	17.7166
2		20.05	20.05	20.0541	0.0206	0.0206	31.2858	40.7114	48.6978
3		51.3342	51.33465	51.3613	0.0529	0.0520	70.2504	83.5303	95.3692
4		–	–	98.0985	–	–	124.7481	141.9056	157.6144
1	0.7	4.0669	4.06694	4.0671	0.0055	0.0045	8.2497	13.9610	18.9222
2		20.5554	20.55552	20.5607	0.0259	0.0253	33.4041	43.1325	52.0916
3		–	54.0152	54.0458	–	0.0566	75.0938	88.9709	102.0832
4		–	–	104.0782	–	–	133.4497	151.4901	168.7619
1	0.9	–	3.6771	3.6739	–	0.0861	9.3628	14.9557	21.2464
2		–	21.55025	21.5562	–	0.0277	37.4963	47.7522	58.5691
3		–	59.18864	59.2227	–	0.0576	84.3795	99.3254	114.8433
4		–	–	115.5110	–	–	150.0512	169.6935	189.9072

are greater than those of the wedge beams. This suggests that the cone beams exhibit greater sensitivity to cross-sectional changes in terms of frequency. Although the frequencies of cone beams are higher than those of wedge beams for other support conditions, the difference is not as pronounced as in the C-F support case.

4.3. Nonuniform cross-section for FG material beams

Next, the beam dimensionless natural frequencies are presented with nonuniform cross-sections and FGMs.

The results for wedge beams with different support conditions are presented in Tables 8 to 11. The material gradation in the tables follows (23). The material properties are provided in (22). The nonuniform cross-sectional area and moment of inertia of the beams shown in the tables can be defined using (25) and (26) for tapered and cone beams, respectively.

$$\frac{A}{A_0} = 1+\alpha x, \qquad \frac{I}{I_0} = (1+\alpha x)^3, \tag{25}$$

$$\frac{A}{A_0} = (1+\alpha x)^2, \qquad \frac{I}{I_0} = (1+\alpha x)^4. \tag{26}$$

Figure 6 illustrates the variation of the cross-sectional geometry of nonuniform FG beams with respect to the parameter α. When $\alpha = -0.2$, the cross-section is wider at the left end and gradually tapers toward the right end. Conversely, when $\alpha = 0.2$, the left end of the beam has a smaller cross-sectional area compared to the right end. This figure clarifies the geometric influence of the parameter α on the beam shape, providing a clearer interpretation of the corresponding tables and results obtained for different taper configurations.

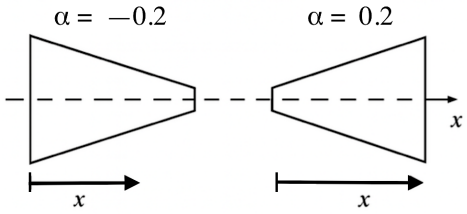

Fig. 6. Cross-sectional variation of nonuniform FG beams with respect to the parameter α

In Table 8, the first frequencies for the C-F condition are compared with those from the literature, while the second, third, and fourth frequencies are predicted in this study. For the remaining support conditions, the predicted results for the P-P, C-P, and C-C cases are provided in Tables 9, 10, and 11, respectively.

Table 8 presents the calculated dimensionless natural frequency values for a C-F wedge beam. The results obtained using the Haar wavelet method show excellent agreement with those of Hein and Feklistova [8]. As the cross-sectional variation α increases, the first frequency values decrease, while the others increase. Furthermore, as the coefficient of the material properties increases, the frequency values also increase.

Figure 7 and Table 8 present the first four DNFs of axially FG tapered C-F beam as functions of the cross-section (α) and the material gradient (γ). The three-dimensional bar plot confirms that the frequency values are more sensitive to geometric variation than the material gradation. The most significant frequency increments are observed at higher modes, particularly in the fourth natural frequency, where the influence of the cross-sectional variation parameter (α) becomes most pronounced, demonstrating its dominant role in shaping the dynamic behavior of the tapered FG beam.

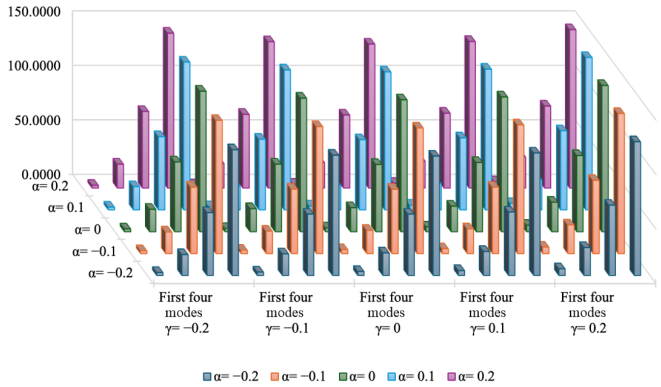

Fig. 7. The first four DNFs of the axially FG tapered C-F beam

Figure 8 illustrates the first and second mode shapes of an axially FG tapered beam with C-F support conditions for various combinations of the cross-section α and the material gradation γ. The upper plot presents the complete mode-shape distribution along the beam axis, while the lower magnified view highlights the local variations around the half-length of the beam. When the cross-sectional variation is $\alpha = -0.2$, the beam is thicker near the clamped end and gradually becomes thinner toward the free end. This geometric configuration enhances the stiffness in the fixed region, leading to a reduction in the overall deflection amplitude. In contrast, when $\alpha = 0.2$, the beam is thinner near the clamped end and thickens toward the free end. The reduced stiffness in the fixed region results in greater curvature and higher deflection of amplitudes under identical conditions. When the cross-sectional variation is kept constant, the influence of the material gradation γ on the first natural frequency of the beam is found to be relatively minor, producing only slight variations in the frequency response. As seen from Fig. 8b, in the case of $\gamma = 0.2$, the Zirconium (ceramic phase) is dominant, resulting in higher stiffness of the beam. Consequently, the smallest amplitudes occur under the influence of this material gradation. The largest amplitudes, where the mode shapes curve toward the right side, are observed for $\gamma = -0.2$, corresponding to the aluminum-rich configuration. The maximum amplitude reaches approximately -1 for $\gamma = -0.2$, is $\alpha = -0.2$ around the half-length of the beam. As a result, both modes show that the geometric variation parameter α causes the greatest change in deflections in the beam mid-region, independent of the material. This difference, which occurs around the beam mid-region, is clearly visible in Fig. 8. In other words, geometric variation is more dominant than material gradation.

Table 8
The first four DNFs of the axially FG tapered C-F beam

n		γ	α				
		−0.2	−0.1	0	0.1	0.2	
1	Present	−0.2	2.6468	2.6051	2.5691	2.5378	2.5102
	[8]		2.6468	2.6051	2.5691	2.5378	2.5102
	Dev. (%)		0.0000	0.0000	0.0000	0.0000	0.0000
2	Present		19.1186	19.8465	20.5526	21.2393	21.9088
3	Present		57.6423	60.8953	64.0790	67.2030	70.2748
4	Present		115.3453	122.2593	129.0158	135.6368	142.1400
1	Present	−0.1	3.0553	3.0103	2.9716	2.9378	2.9081
	[8]		3.0553	3.0103	2.9716	2.9378	2.9081
	Dev. (%)		0.0000	0.0000	0.0000	0.0000	0.0000
2	Present		19.7715	20.4934	21.1936	21.8748	22.5387
3	Present		56.2061	59.1563	62.0349	64.8516	67.6140
4	Present		110.3205	116.5186	122.5591	128.4641	134.2508
1	Present	0	3.6085	3.5589	3.5162	3.4789	3.4460
	[8]		3.6085	3.5589	3.5162	3.4789	3.4460
	Dev. (%)		0.0000	0.0000	0.0000	0.0000	0.0000
2	Present		20.6269	21.3441	22.0403	22.7178	23.3787
3	Present		56.2257	59.0140	61.7313	64.3873	66.9895
4	Present		109.4287	115.3006	121.0170	126.5997	132.0657
1	Present	0.1	4.4492	4.3922	4.3430	4.2999	4.2618
	[8]		4.4492	4.3922	4.3430	4.2999	4.2618
	Dev. (%)		0.0000	0.0000	0.0000	0.0000	0.0000
2	Present		21.9940	22.7132	23.4127	24.0946	24.7604
3	Present		58.1222	60.8485	63.5049	66.1008	68.6434
4	Present		112.3046	118.0567	123.6544	129.1189	134.4672
1	Present	0.2	6.0214	5.9518	5.8909	5.8372	5.7893
	[8]		6.0214	5.9518	5.8909	5.8372	5.7893
	Dev. (%)		0.0000	0.0000	0.0000	0.0000	0.0000
2	Present		25.5802	26.3297	27.0624	27.7795	28.4821
3	Present		64.4060	67.1960	69.9186	72.5820	75.1930
4	Present		122.6895	128.5522	134.2614	139.8380	145.2983

Table 9 shows the effects of cross-sectional and material variations on the dimensionless natural frequency for a tapered P-P beam, a condition not previously addressed in the literature. When there is no cross-section ($\alpha = 0$), the first frequencies yield identical results regardless of the material parameter, i.e., the material does not affect the frequency at this stage. While the material property coefficient γ does not influence the first frequencies, its impact increases at higher-order frequencies. Additionally, as cross-sectional variation increases for a given material gradient, the frequency values also increase.

Figure 9 is the visual representation of Table 9. Although the α and γ do not cause significant variations in the first two frequencies; a remarkable increase is observed in the third and fourth frequencies. The highest frequency values occur in the fourth mode. The case with $\gamma = -0.2$, $\alpha = 0.2$ yields the maximum frequency value of 190.9837, followed by the case $\gamma = 0.2$, $\alpha = 0.2$, with a frequency of 187.7511.

It is shown in the mode shapes corresponding to the first and second natural frequencies of the P-P beam in Fig. 10. In Fig. 10a, the first mode exhibits a one curvature bending form with only small location variations of the maximum deflection points on the beam axis for different combinations of the parameters γ and α. Figure 10b shows that the second-mode shape displays greater sensitivity of the gradation of the material and the section geometry in terms of curvature and amplitude of deflection. As expected, in the absence of material gradation ($\gamma = 0$),

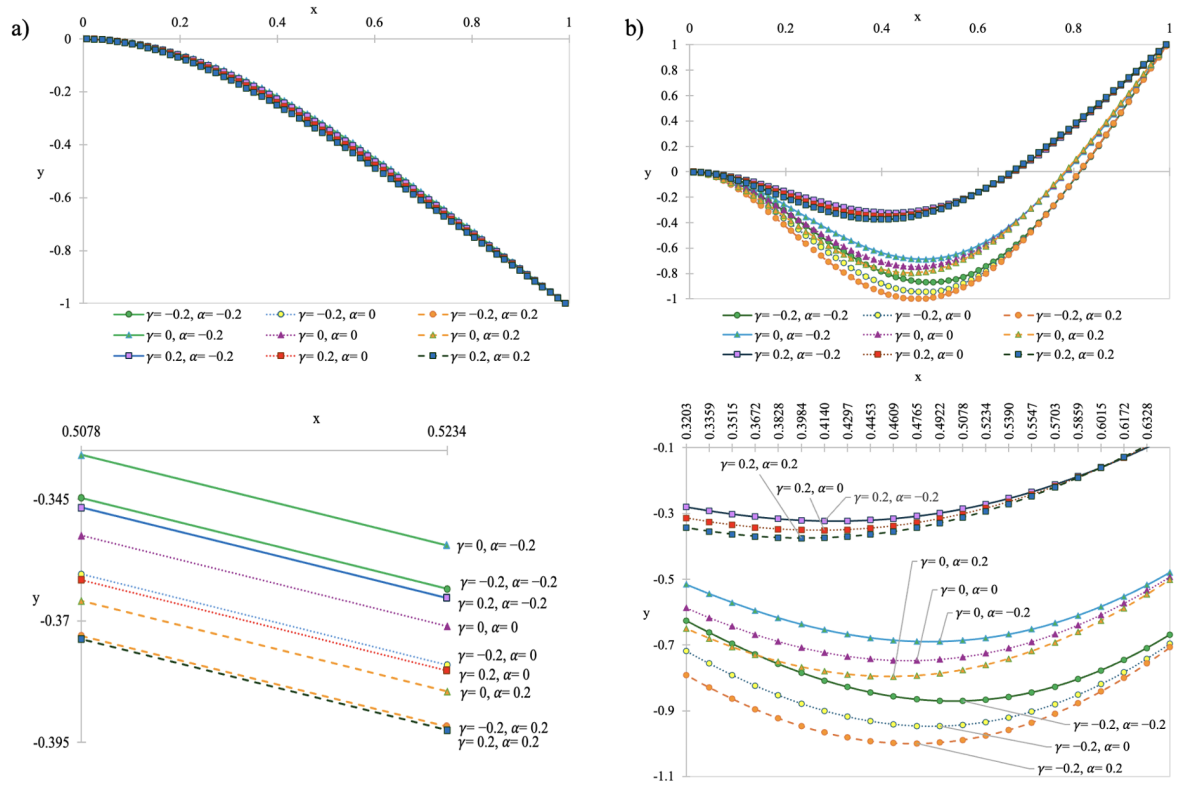

Fig. 8. The mode shape of the axially FG tapered C-F beam: a) The first mode shape, b) The second mode shape

Table 9
The first four DNFs of the axially FG tapered P-P beam

n	γ	α				
		−0.2	−0.1	0	0.1	0.2
1	−0.2	8.8641	9.3768	9.8701	10.3468	10.8091
2		37.7113	40.1513	42.5472	44.9058	47.2321
3		85.8993	91.4044	96.7948	102.0875	107.2958
4		153.1833	162.9310	172.4599	181.8024	190.9837
1	−0.1	8.8553	9.3724	9.8701	10.3513	10.8182
2		35.8973	38.0739	40.2051	42.2974	44.3562
3		80.86245	85.7025	90.4663	95.1325	99.7142
4		143.7263	152.3835	160.8256	169.0842	177.1840
1	0	8.8464	9.3679	9.8701	10.3558	10.8271
2		35.4514	37.4916	39.4863	41.4422	43.3644
3		79.7643	84.3723	88.8666	93.2638	97.5770
4		141.8314	150.0428	158.0406	165.8560	173.5135
1	0.1	8.8374	9.3634	9.8701	10.3602	10.8360
2		36.2994	38.2750	40.2051	42.0964	43.9541
3		81.5814	86.0810	90.4663	94.7540	98.9573
4		144.9444	152.9925	160.8256	168.4752	175.9659
1	0.2	8.8284	9.3589	9.8701	10.3647	10.8449
2		38.7076	40.6492	42.5472	44.4079	46.2360
3		87.8973	92.4032	96.7948	101.0888	105.2980
4		156.4162	164.5471	172.4599	180.1864	187.7511

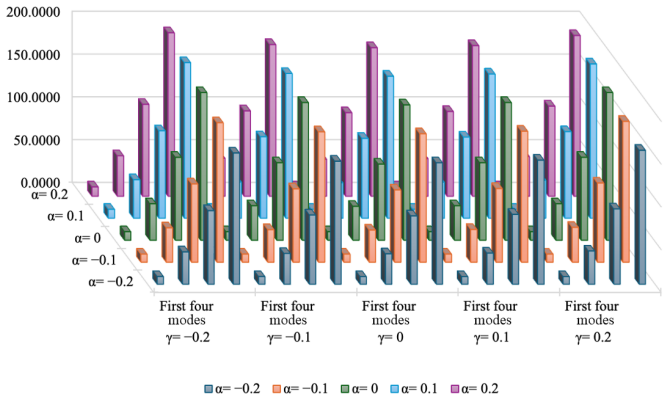

Fig. 9. The first four DNFs of the axially FG tapered P-P beam

the cross-section change parameter has an asymmetric structure due to symmetric support conditions. Under the influence of material gradation, as γ increases from −0.2 to positive values, the proportion of the aluminum-rich region decreases while the ceramic phase increases, resulting in higher stiffness and thus reduced deflection in this region. In summary, increases in both α and γ enhance the mode asymmetry. The largest deformations occur for the asymmetric cases $\gamma = 0.2$, $\alpha = -0.2$ and $\gamma = -0.2$, $\alpha = 0.2$.

The results for the C-P and C-C tapered beams are presented in Tables 10 and 11. We observe that if the cross-sectional variation parameter increases, the frequency also increases. The same relationship is observed between frequencies for the coefficient

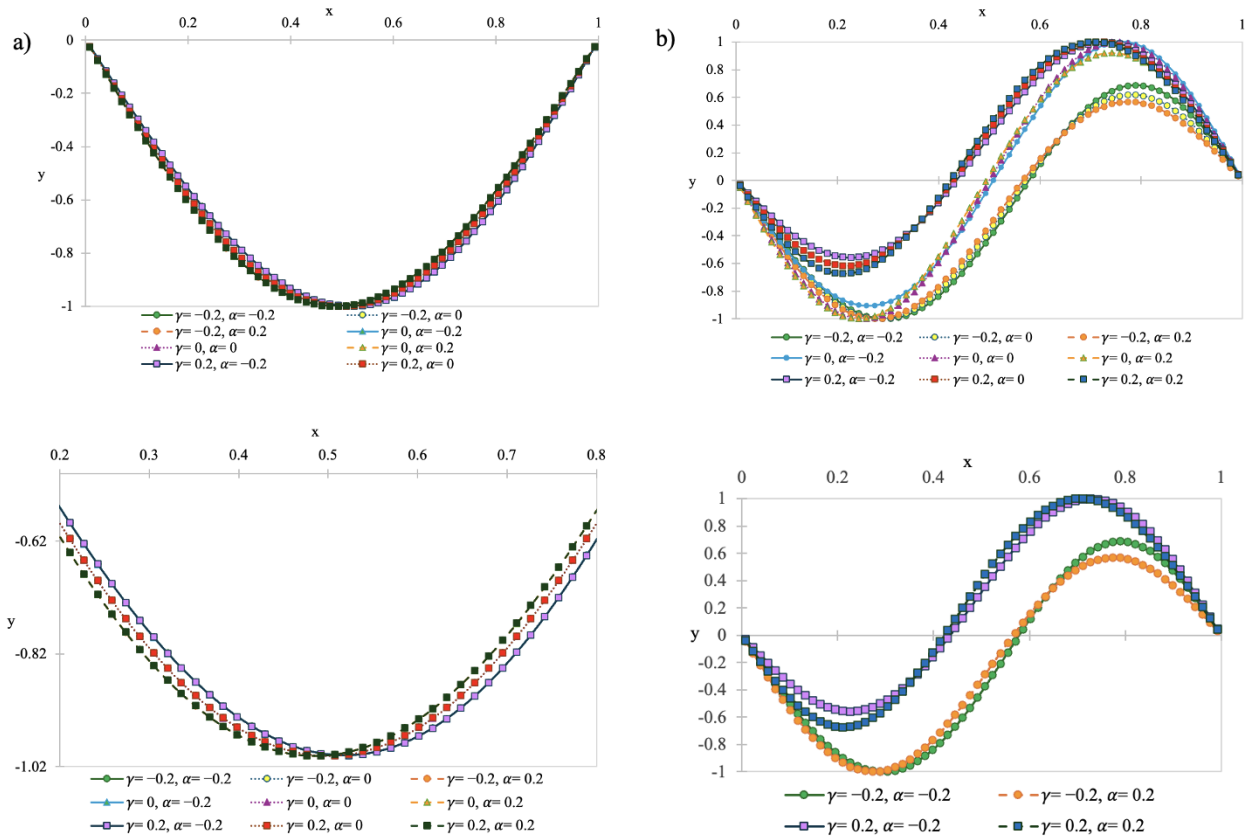

Fig. 10. The mode shape of the axially FG tapered P-P beam: a) The first mode shape, b) The second mode shape

of material properties. However, the influence of material variation on frequency is not as pronounced as that of cross-sectional variation.

Table 11 presents frequencies of a nonuniform tapered C-C beam. When there is no cross-sectional variation ($\alpha = 0$), the frequency values are identical due to the symmetry of the supports for absolute values of γ. In general, while the effects of changes in material parameters on the lower-order frequencies are minimal, their influence increases for higher-order frequencies.

Table 12 shows the results for the FGs for the cone C-F beam. As the cross-sectional variation parameter shifts from −0.2 to +0.2, the first frequency values decrease, while higher-order frequencies increase. Additionally, for any cross-sectional variation, the gradation of the material properties increases the frequency values. This relationship can be observed by reviewing each column in Table 12.

Table 12 and Fig. 11 illustrate the influence of the parameters α and γ on the first four natural frequencies. While the variation is limited in the first two modes, a significant increase is observed in the third and fourth modes. The highest value occurs in the fourth mode because of cross-sectional variation.

Figure 12 shows the first and second vibration modes of the FG cone C-F beam. The first mode exhibits classical cantilever behavior, with zero displacement and slope at the clamped end and maximum deflection at the free end. The influence of material gradation remains nearly identical for $\alpha = 0.2$ and $\alpha = 0$,

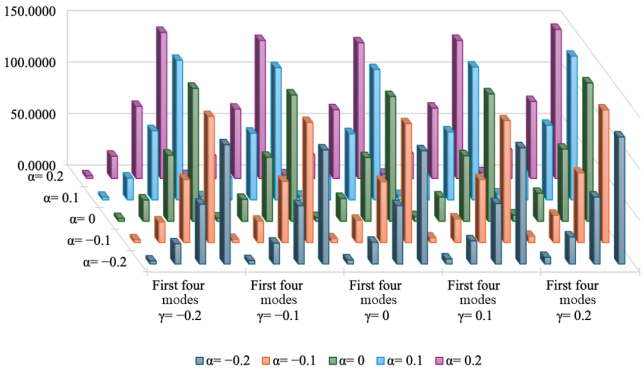

Fig. 11. The first four DNFs of the axially FG cone C-F beam

while a more noticeable deviation is observed for $\alpha = -0.2$. In the second mode, a single nodal point appears, as expected; however, the position of this node and the amplitude distribution vary depending on the values of α and γ. Compared to the reference case where both parameters are zero, the combination $\gamma = -0.2$, $\alpha = 0.2$ yields the maximum deflection amplitude, approximately 25% higher. In contrast, when the ceramic phase is dominant ($\gamma = 0.2$), the increased stiffness restricts the vibration motion, resulting in lower amplitude oscillations.

In Table 13, the increase in cross-sectional variation increases all frequency values for the nonuniform cone P-P beam, while the material directional properties increase sensitivity.

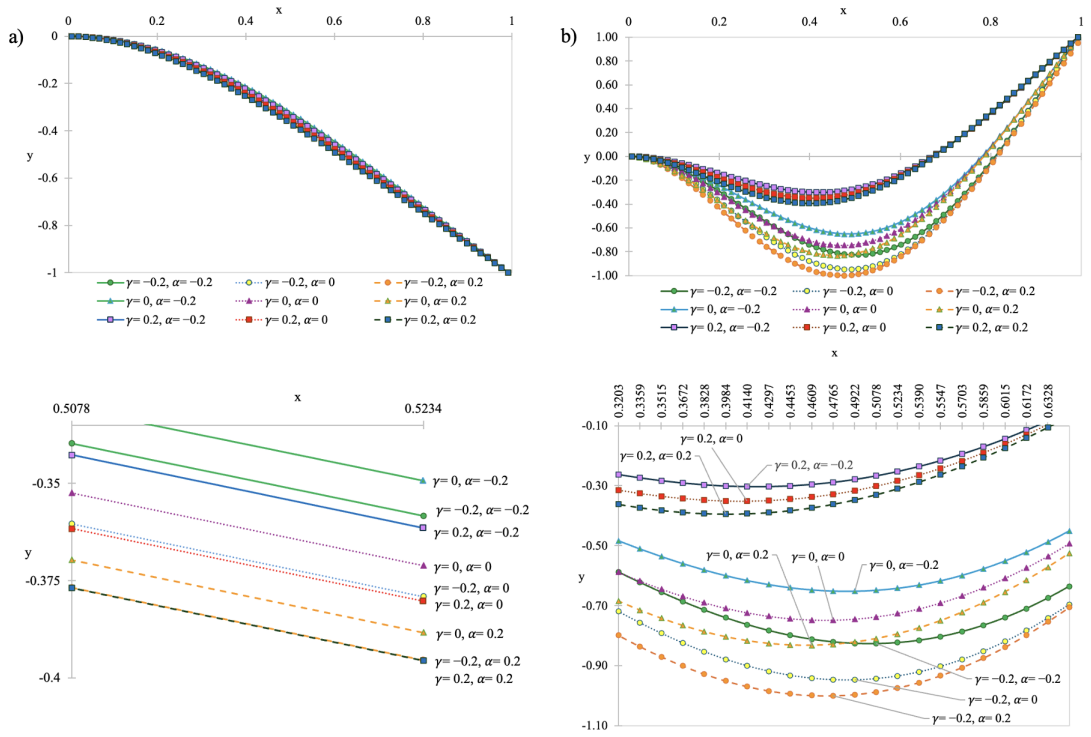

Fig. 12. The mode shape of the axially FG cone C-F beam: a) The first mode shape, b) The second mode shape

Table 10
The first four DNFs of the axially FG tapered C-P beam

n	γ	α				
		−0.2	−0.1	0	0.1	0.2
1	−0.2	13.0570	13.6461	14.2126	14.7598	15.2902
2		46.0658	48.8270	51.5260	54.1719	56.7719
3		98.8190	104.9351	110.9079	116.7584	122.5029
4		170.9248	181.5927	192.0038	202.1953	212.1965
1	−0.1	13.6238	14.2162	14.7860	15.3364	15.8701
2		45.2089	47.7393	50.2045	52.6138	54.9747
3		94.7746	100.2818	105.6446	110.8838	116.0158
4		162.2826	171.8419	181.1470	190.2350	199.1343
1	0	14.2580	14.8497	15.4191	15.9696	16.5035
2		45.2532	47.6472	49.9758	52.2483	54.4722
3		93.9966	99.2187	104.2976	109.2538	114.1037
4		160.5014	169.5862	178.4194	187.0374	195.4687
1	0.1	14.9752	15.5603	16.1243	16.6702	17.2003
2		46.5598	48.8898	51.1544	53.3629	55.5228
3		96.2657	101.3768	106.3442	111.1887	115.9266
4		164.1122	173.0274	181.6898	190.1362	198.3951
1	0.2	15.7888	16.3597	16.9114	17.4467	17.9676
2		49.9393	52.2394	54.4758	56.6576	58.7919
3		103.8399	108.9741	113.9641	118.8307	123.5899
4		177.1289	186.1505	194.9156	203.4613	211.8162

Table 11
The first four DNFs of the axially FG tapered C-C beam

n	γ	α				
		−0.2	−0.1	0	0.1	0.2
1	−0.2	19.7831	21.0909	22.3710	23.6277	24.8643
2		57.3001	61.0236	64.6623	68.2286	71.7324
3		114.8364	122.2059	129.3991	136.4423	143.3554
4		191.7021	203.9167	215.8326	227.4939	238.9346
1	−0.1	19.9298	21.1668	22.3738	23.5553	24.7147
2		55.7053	59.1031	62.4128	65.6474	68.8167
3		109.7002	116.3380	122.7990	129.1092	135.2887
4		181.6632	192.6201	203.2821	213.6926	223.8850
1	0	20.0789	21.2422	22.3747	23.4810	24.5645
2		55.3514	58.5634	61.6873	64.7359	67.7194
3		108.5347	114.8373	120.9642	126.9413	132.7884
4		179.4758	189.9012	200.0340	209.9171	219.5839
1	0.1	20.2296	21.3166	22.3738	23.4054	24.4149
2		56.3036	59.4023	62.4128	65.3482	68.2184
3		110.6676	116.8218	122.7990	128.6254	134.3212
4		183.1264	193.3518	203.2821	212.9609	222.4217
1	0.2	20.3807	21.3895	22.3710	23.3292	24.2669
2		58.7706	61.7588	64.6623	67.4935	70.2619
3		117.4146	123.4948	129.3991	135.1533	140.7773
4		195.6648	205.8979	215.8326	225.5127	234.9720

Table 12
The first four DNFs of the axially FG cone C-F beam

n	γ	α				
		−0.2	−0.1	0	0.1	0.2
1	−0.2	2.8367	2.6932	2.5691	2.4606	2.3646
2		19.5442	20.0555	20.5526	21.0358	21.5057
3		58.0335	61.0808	64.0790	67.0346	69.9527
4		115.7337	122.4420	129.0158	135.4735	141.8300
1	−0.1	3.2700	3.1101	2.9716	2.8501	2.7423
2		20.1983	20.7021	21.1936	21.6729	22.1402
3		56.6120	59.3493	62.0349	64.6752	67.2755
4		110.7272	116.7108	122.5591	128.2906	133.9199
1	0	3.8554	3.6739	3.5162	3.3774	3.2539
2		21.0625	21.5562	22.0403	22.5141	22.9778
3		56.6633	59.2227	61.7313	64.1953	66.6195
4		109.8723	115.5110	121.0170	126.4081	131.6986
1	0.1	4.7404	4.5283	4.3430	4.1791	4.0328
2		22.4600	22.9391	23.4127	23.8794	24.3384
3		58.6123	61.0827	63.5049	65.8844	68.2256
4		112.8093	118.2969	123.6544	128.8989	134.0442
1	0.2	6.3745	6.1180	5.8909	5.6881	5.5053
2		26.1584	26.6083	27.0624	27.5171	27.9699
3		65.0252	67.4919	69.9186	72.3084	74.6644
4		123.3309	128.8578	134.2614	139.5568	144.7561

Table 13
The first four DNFs of the axially FG cone P-P beam

n	γ	α				
		−0.2	−0.1	0	0.1	0.2
1	−0.2	8.8954	9.3983	9.8701	10.3155	10.7381
2		37.6867	40.1333	42.5472	44.9337	47.2967
3		85.8503	91.3710	96.7948	102.1362	107.4066
4		153.1179	162.8879	172.4599	181.8634	191.1215
1	−0.1	8.8601	9.3806	9.8701	10.3333	10.7738
2		35.8869	38.0634	40.2051	42.3172	44.4038
3		80.8123	85.6882	90.4663	95.1609	99.7833
4		143.7145	152.3681	160.8256	169.1159	177.2615
1	0	8.8246	9.3628	9.8701	10.3511	10.8093
2		35.4711	37.4963	39.4863	41.4464	43.3806
3		79.7949	84.3795	88.8666	93.2704	97.6020
4		141.8668	150.0512	158.0406	165.8636	173.5425
1	0.1	8.7891	9.3450	9.8701	10.3689	10.8448
2		36.3508	38.2952	40.2051	42.0854	43.9400
3		81.6562	86.1101	90.4663	94.7390	98.9395
4		145.0286	153.0250	160.8256	168.4590	175.9475
1	0.2	8.7535	9.3271	9.8701	10.3867	10.8802
2		38.7763	40.6777	42.5472	44.3894	46.2074
3		88.0145	92.4526	96.7948	101.0546	105.2429
4		156.5614	164.6090	172.4599	180.1424	187.6785

Figure 13 and Table 13 show that the influence of the parameters α and γ on the FG cone beam with P-P boundary conditions exhibits a trend similar to that observed in tapered beams. In the third and fourth modes, both parameters lead to considerably higher natural frequency values.

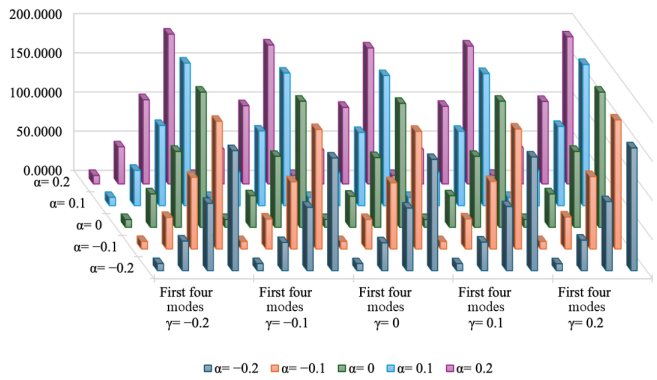

Fig. 13. The first four DNFs of the axially FG cone P-P beam

Figure 14 presents the first and second mode shapes of the FG cone P-P beam, which exhibit dynamic characteristics comparable to those of tapered FG beams, nearly identical. In Fig. 14a, the first mode shape displays a slight asymmetry arising from the combined influence of the cross-sectional variation parameter α and the material gradient parameter γ. In contrast, Fig. 14b demonstrates that the second mode shape is more strongly affected by the material gradation, indicating a greater sensitivity of higher modes to variations in material distribution. For identical material gradient values, the difference between the frequency responses corresponding to $\alpha = -0.2$ and $\alpha = 0.2$ becomes more pronounced. At $\gamma = 0.2$, the minimum deflection point is recorded as −0.5257 for $\alpha = -0.2$ and −0.7073 for $\alpha = 0.2$.

These findings suggest that in FG cone beams, the cross-sectional variation exerts a more dominant influence on the dynamic response than the material gradation, particularly for higher vibration modes.

Table 14 displays the first four frequencies corresponding to variations in cross-sectional and material properties for the nonuniform cone C-P beam. The first frequency consistently increases with the increase in both the cross-section and material property parameters. While there is no uniform increase in the absolute values for material property changes, the table shows that all frequency values generally increase as the cross-sectional variation becomes more pronounced.

Table 15 presents an analysis of the frequency values of a nonuniform cone C-C beam. The results indicate that frequency values increase as the degree of cross-sectional variation in-

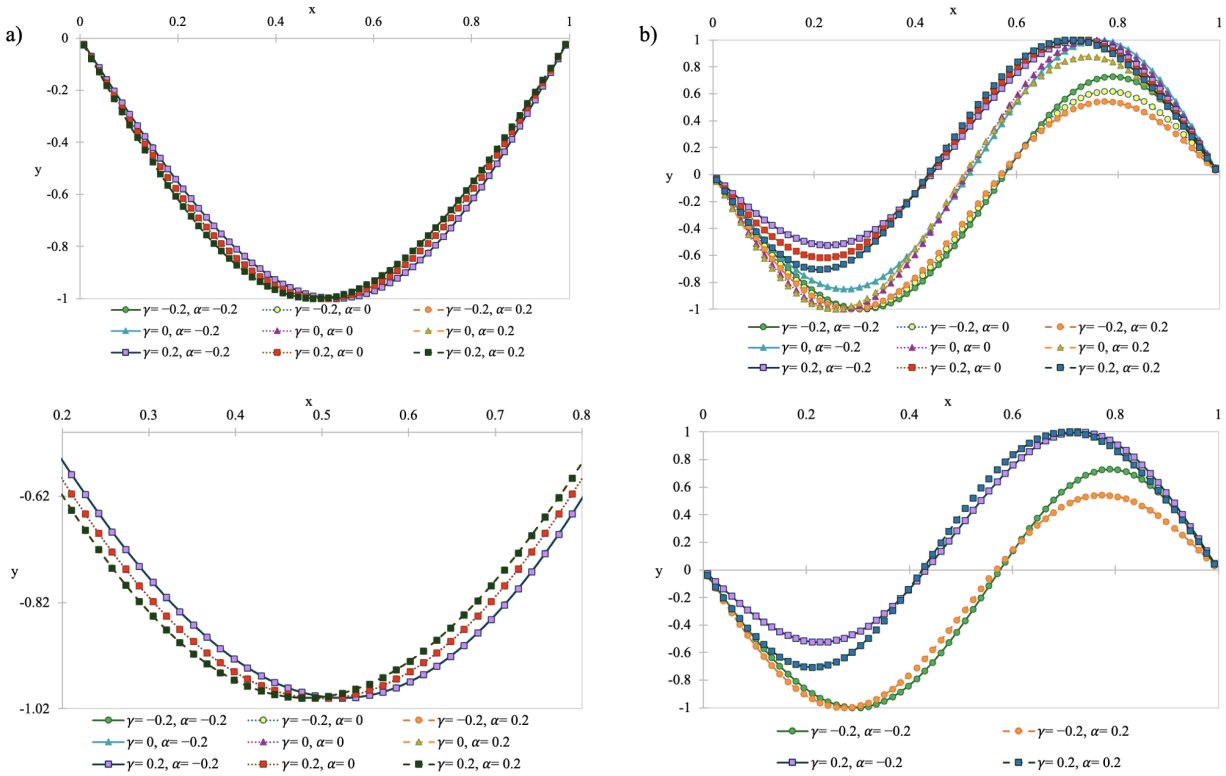

Fig. 14. The mode shape of the axially FG cone P-P beam: a) The first mode shape, b) The second mode shape

Table 14
The first four DNFs of the axially FG cone C-P beam

n	γ	α				
		−0.2	−0.1	0	0.1	0.2
1	−0.2	13.2673	13.7524	14.2126	14.6514	15.0715
2		46.2512	48.9135	51.5260	54.0964	56.6308
3		99.0030	105.0191	110.9079	116.6882	122.3746
4		171.1075	181.6756	192.0038	202.1273	212.0735
1	−0.1	13.8360	14.3227	14.7860	15.2291	15.6544
2		45.4091	47.8335	50.2045	52.5301	54.8165
3		94.9766	100.3753	105.6446	110.8033	115.8660
4		162.4854	171.9352	181.1470	190.1556	198.9877
1	0	14.4708	14.9557	15.4191	15.8639	16.2923
2		45.4747	47.7522	49.9758	52.1533	54.2910
3		94.2247	99.3254	104.2976	109.1598	113.9267
4		160.7321	169.6935	178.4194	186.9438	195.2935
1	0.1	15.1862	15.6647	16.1243	16.5675	16.9958
2		46.8087	49.0084	51.1544	53.2545	55.3149
3		96.5303	101.5015	106.3442	111.0770	115.7144
4		164.3829	173.1544	181.6898	190.0234	198.1817
1	0.2	15.9944	16.4605	16.9114	17.3486	17.7733
2		50.2137	52.3701	54.4758	56.5380	58.5622
3		104.1520	109.1216	113.9641	118.6974	123.3357
4		177.4634	186.3083	194.9156	203.3194	211.5461

Table 15
The first four DNFs of the axially FG cone C-C beam

n	γ	α				
		−0.2	−0.1	0	0.1	0.2
1	−0.2	19.7789	21.0841	22.3710	23.6427	24.9016
2		57.2889	61.0113	64.6623	68.2527	71.7908
3		114.8235	122.1922	129.3991	136.4684	143.4187
4		191.6880	203.9024	215.8326	227.5208	238.9996
1	−0.1	19.9366	21.1655	22.3738	23.5647	24.7407
2		55.7121	59.1001	62.4128	65.6614	68.8544
3		109.7071	116.3347	122.7990	129.1242	135.3288
4		181.6698	192.6166	203.2821	213.7078	223.9256
1	0	20.0970	21.2464	22.3747	23.4848	24.5792
2		55.3754	58.5691	61.6873	64.7410	67.7390
3		108.5601	114.8433	120.9642	126.9467	132.8092
4		179.5013	189.9072	200.0340	209.9225	219.6048
1	0.1	20.2590	21.3264	22.3738	23.4037	24.4185
2		56.3458	59.4169	62.4128	65.3446	68.2207
3		110.7125	116.8373	122.7990	128.6216	134.3235
4		183.1718	193.3675	203.2821	212.9568	222.4236
1	0.2	20.4215	21.4049	22.3710	23.3220	24.2595
2		58.8340	61.7834	64.6623	67.4806	70.2461
3		117.4833	123.5216	129.3991	135.1390	140.7594
4		195.7350	205.9254	215.8326	225.4978	234.9530

creases. If there is no cross-sectional variation ($\alpha = 0$), as shown in Table 15 row 5, the frequencies are identical for the absolute values of the material variation coefficient. In general, when analyzed in terms of the effect of material variation, despite the influence of symmetrical supports, the cone nature of the beam results in closely aligned absolute and frequency values.

5. CONCLUSIONS

In this study, the flexural free vibration of axially functionally graded Euler-Bernoulli beams was investigated using the Haar wavelet method. The governing equations under four different boundary conditions were derived and efficiently solved. The accuracy of the method was verified through direct comparisons with benchmark results from the literature, confirming its reliability for free vibration analysis.

Beyond validation, the study extended the analysis to tapered and cone-shaped beams with axial gradation in material properties, for which no prior investigations have been reported. The results demonstrated that geometric variations in the cross-section have a more dominant effect on natural frequencies than material gradation. In the cases examined, the frequencies of taper and cone beams are nearly identical because the effect of beam width on the sectional moment of inertia is negligible.

REFERENCES

[1] A.J. Markworth, K.S. Ramesh, and W.P. Parks, "Modelling Studies Applied to Functionally Graded Materials," *J. Mater. Sci.*, vol. 30, pp. 2183–2193, 1995, doi: 10.1007/bf01184560.

[2] B.V. Sankar, "An elasticity solution for functionally graded beams," *Compos. Sci. Technol.*, vol. 61, pp. 689–696, 2001, doi: 10.1016/S0266-3538(01)00007-0.

[3] L. Chen and T. Goto, "Functionally Graded Materials," in *Handbook of Advanced Ceramics*, Elsevier, 2003, pp. 445–464. doi: 10.1016/B978-012654640-8/50043-2.

[4] X.F. Li, "A unified approach for analyzing static and dynamic behaviors of functionally graded Timoshenko and Euler-Bernoulli beams," *J. Sound Vib.*, vol. 318, no. 4–5, pp. 1210–1229, Dec. 2008, doi: 10.1016/j.jsv.2008.04.056.

[5] B. Kılıç and Ö. Özdemir, "Vibration and stability analyses of functionally graded beams," *Arch. Mech. Eng.*, vol. 68, no. 1, pp. 93–113, 2021, doi: 10.24425/ame.2021.137043.

[6] V. Birman and L.W. Byrd, "Modeling and Analysis of Functionally Graded Materials and Structures," *Appl. Mech. Rev.*, vol. 60, no. 5, pp. 195–216, Sept. 2007, doi: 10.1115/1.2777164.

[7] S.A. Sina, H.M. Navazi, and H. Haddadpour, "An analytical method for free vibration analysis of functionally graded beams," *Mater. Des.*, vol. 30, no. 3, pp. 741–747, Mar. 2009, doi: 10.1016/j.matdes.2008.05.015.

[8] H. Hein and L. Feklistova, "Computationally efficient delamination detection in composite beams using Haar wavelets," *Mech. Syst. Signal Proces.*, vol. 25, no. 6, pp. 2257–2270, Aug. 2011, doi: 10.1016/j.ymssp.2011.02.003.

[9] J. Kim and G.H. Paulino, "Finite element evaluation of mixed mode stress intensity factors in functionally graded materials," *Int. J. Num. Meth. Eng.*, vol. 53, no. 8, pp. 1903–1935, Mar. 2002, doi: 10.1002/nme.364.

[10] D.S. Mashat, E. Carrera, A.M. Zenkour, S.A. Al Khateeb, and M. Filippi, "Free vibration of FGM layered beams by various theories and finite elements," *Compos. Part B-Eng.*, vol. 59, pp. 269–278, Mar. 2014, doi: 10.1016/j.compositesb.2013.12.008.

[11] A. Mortensen and S. Suresh, "Functionally graded metals and metal-ceramic composites: Part 1 Processing," *Int. Mater. Rev.*, vol. 40, no. 6, pp. 239–265, Jan. 1995, doi: 10.1179/imr.1995.40.6.239.

[12] M. Koizumi, "The concept of FGM," *Ceram. Trans.-Functionally Gradient Mater.*, vol. 34, pp. 3–10, 1993.

[13] A.J. Ruys and B.A. Sutton, "Metal-ceramic functionally graded materials (FGMs)," in *Metal-Reinforced Ceramics*, Elsevier, 2021, pp. 327–359, doi: 10.1016/B978-0-08-102869-8.00009-4.

[14] S. Naguleswaran, "A Direct Solution for the Transverse Vibration of Euler-Bernoulli Wedge and Cone Beams," *J. Sound Vib.*, vol. 172, no. 3, pp. 289–304, May 1994, doi: 10.1006/jsvi.1994.1176.

[15] Y. Huang and X.-F. Li, "A new approach for free vibration of axially functionally graded beams with non-uniform cross-section," *J. Sound Vib.*, vol. 329, no. 11, pp. 2291–2303, May 2010, doi: 10.1016/j.jsv.2009.12.029.

[16] Ü. Lepik and H. Hein, *Mathematical Engineering Haar Wavelets with Applications*, vol. 4. Springer, 2014. [Online]. Available: http://www.springer.com/series/8445

[17] Y.K. Cheung and C.I. Wu, "Free vibrations of thick, layered cylinders having finite length with various boundary conditions," *J. Sound Vib.*, vol. 24, no. 2, pp. 189–200, Sept. 1972, doi: 10.1016/0022-460X(72)90948-0.

[18] K.P. Soldatos and V.P. Hadjigeorgiou, "Three-dimensional solution of the free vibration problem of homogeneous isotropic cylindrical shells and panels," *J. Sound Vib.*, vol. 137, no. 3, pp. 369–384, Mar. 1990, doi: 10.1016/0022-460X(90)90805-A.

[19] C.T. Loy, K.Y. Lam, and J.N. Reddy, "Vibration of functionally graded cylindrical shells," *Int. J. Mech. Sci.*, vol. 41, no. 3, pp. 309–324, Mar. 1999, doi: 10.1016/S0020-7403(98)00054-X.

[20] S.C. Pradhan, C.T. Loy, K.Y. Lam, and J.N. Reddy, "Vibration characteristics of functionally graded cylindrical shells under various boundary conditions," *Appl. Acoust.*, vol. 61, no. 1, pp. 111–129, Sept. 2000, doi: 10.1016/S0003-682X(99)00063-8.

[21] S.S. Vel and R.C. Batra, "Three-dimensional exact solution for the vibration of functionally graded rectangular plates," *J. Sound Vib.*, vol. 272, no. 3–5, pp. 703–730, May 2004, doi: 10.1016/S0022-460X(03)00412-7.

[22] M. Arefi, E. Mohammad-Rezaei Bidgoli, R. Dimitri, and F. Tornabene, "Free vibrations of functionally graded polymer composite nanoplates reinforced with graphene nanoplatelets," *Aerosp. Sci. Technol.*, vol. 81, pp. 108–117, Oct. 2018, doi: 10.1016/j.ast.2018.07.036.

[23] N. Vasiraja and P. Nagaraj, "The effect of material gradient on the static and dynamic response of layered functionally graded material plate using finite element method," *Bull. Pol. Acad. Sci. Tech. Sci.*, vol. 67, no. 4, pp. 827–838, 2019, doi: 10.24425/bpasts.2019.130191.

[24] Y.S. Li and B.L. Liu, "Thermal buckling and free vibration of viscoelastic functionally graded sandwich shells with tunable auxetic honeycomb core," *Appl. Math. Model.*, vol. 108, pp. 685–700, Aug. 2022, doi: 10.1016/j.apm.2022.04.019.

[25] P.T. Thang, D.T.T. Do, T.-T. Nguyen, J. Lee, and T. Nguyen-Thoi, "Free vibration characteristic analysis of functionally graded shells with porosity and neutral surface effects," *Ocean*

Eng., vol. 255, p. 111377, July 2022, doi: 10.1016/j.oceaneng.2022.111377.

[26] Q. Zang, J. Liu, W. Ye, F. Yang, C. Hao, and G. Lin, "Static and free vibration analyses of functionally graded plates based on an isogeometric scaled boundary finite element method," *Compos. Struct.*, vol. 288, p. 115398, May 2022, doi: 10.1016/j.compstruct.2022.115398.

[27] S. Marzavan and V. Nastasescu, "Free Vibration Analysis of a Functionally Graded Plate by Finite Element Method," *Ain Shams Eng. J.*, vol. 14, no. 8, p. 102024, Aug. 2023, doi: 10.1016/j.asej.2022.102024.

[28] M. Mishra, C.K. Srivastav, and S. Kumar, "Free vibration analysis using dynamic stiffness method and first-order shear deformation theory for a functionally graded material plate," *Mater. Today-Proc.*, vol. 98, pp. 7–15, 2024, doi: 10.1016/j.matpr.2023.08.295.

[29] D. Gogoi, M.K. Pandit, and A.K. Pradhan, "Free vibration behavior in functionally graded material plates with dual efficient quadrilateral finite elements," *Mech. Based Des. Struct. Mach.*, vol. 52, no. 12, pp. 9830–9857, Dec. 2024, doi: 10.1080/15397734.2024.2348104.

[30] C.-C. Hong, "Advanced Vibration of Functionally Graded Material Coupled Plates and Circular Shells with Four Layers," *Fibers*, vol. 13, no. 3, p. 32, Mar. 2025, doi: 10.3390/fib13030032.

[31] A. Radaković, D. Čukanović, A. Nešović, P. Knežević, M.T. Djordjević, and G. Bogdanović, "Free Vibration Analysis of Porous FGM Plates on Elastic Foundations with Temperature-Dependent Material Properties," *Mathematics*, vol. 13, no. 18, p. 2957, Sept. 2025, doi: 10.3390/math13182957.

[32] J. Zhang *et al.*, "Free vibration solutions of functionally graded plates with various boundary conditions using unified finite integral transform approach," *Eng. Struct.*, vol. 341, p. 120788, Oct. 2025, doi: 10.1016/j.engstruct.2025.120788.

[33] M. Aydogdu and V. Taskin, "Free vibration analysis of functionally graded beams with simply supported edges," *Mater. Des.*, vol. 28, no. 5, pp. 1651–1656, 2007, doi: 10.1016/j.matdes.2006.02.007.

[34] S. Kumar, A. Mitra, and H. Roy, "Geometrically nonlinear free vibration analysis of axially functionally graded taper beams," *Eng. Sci. Technol. Int. J.*, vol. 18, no. 4, pp. 579–593, Dec. 2015, doi: 10.1016/j.jestch.2015.04.003.

[35] P. Sharma and R. Singh, "A numerical study on free vibration analysis of axial FGM beam," *Mater. Today-Proc.*, vol. 44, pp. 1664–1668, 2021, doi: 10.1016/j.matpr.2020.11.827.

[36] M. Turan, E. Uzun Yaylacı, and M. Yaylacı, "Free vibration and buckling of functionally graded porous beams using analytical, finite element, and artificial neural network methods," *Arch. Appl. Mech.*, vol. 93, no. 4, pp. 1351–1372, Apr. 2023, doi: 10.1007/s00419-022-02332-w.

[37] J.-J. Mao, Y.-J. Wang, W. Zhang, M.Q. Wu, Y.Z. Liu, and X.-H. Liu, "Vibration and wave propagation in functionally graded beams with inclined cracks," *Appl. Math. Modelling*, vol. 118, pp. 166–184, June 2023, doi: 10.1016/j.apm.2023.01.035.

[38] L. Zhang, Z. Xu, M. Gao, R. Xu, and G. Wang, "Static, dynamic and buckling responses of random functionally graded beams reinforced by graphene platelets," *Eng. Struct.*, vol. 291, p. 116476, Sept. 2023, doi: 10.1016/j.engstruct.2023.116476.

[39] W. Li, Z. Liu, and S. Chen, "A modified quasi-3D theory and mixed beam element method for static behaviour analysis of functionally graded beams," *Thin-Walled Struct.*, vol. 204, p. 112316, Nov. 2024, doi: 10.1016/j.tws.2024.112316.

[40] C. Tang, G. Dui, and Y. Fu, "Elasticity solutions for functionally graded beams with arbitrary distributed loads," *Compos. Struct.*, vol. 351, pp. 118578, Jan. 2025, doi: 10.1016/j.compstruct.2024.118578.

[41] Y. Huang, H. Liu, and Y. Zhao, "Dynamic Analysis of Non-Uniform Functionally Graded Beams on Inhomogeneous Foundations Subjected to Moving Distributed Loads," *Appl. Sci.*, vol. 13, no. 18, p. 10309, Sept. 2023, doi: 10.3390/app131810309.

[42] D. Cao, B. Wang, W. Hu, and Y. Gao, "Free Vibration of Axially Functionally Graded Beam," in *Mechanics of Functionally Graded Materials and Structures*, IntechOpen, 2020. doi: 10.5772/intechopen.85835.

[43] A. Chakraborty, S. Gopalakrishnan, and J.N. Reddy, "A new beam finite element for the analysis of functionally graded materials," *Int. J. Mech. Sci.*, vol. 45, no. 3, pp. 519–539, Mar. 2003, doi: 10.1016/S0020-7403(03)00058-4.

[44] C.-F. Lu and W.Q. Chen, "Free vibration of orthotropic functionally graded beams with various end conditions," *Struct. Eng. Mech.*, vol. 20, no. 4, pp. 465–476, July 2005, doi: 10.12989/sem.2005.20.4.465.

[45] Y. El Khouddar, A. Adri, O. Outassafte, I. El Hantati, S. Rifai, and R. Benamar, "Analysis of Geometrically Non-Linear Free Vibrations of Functional Graded Beams in a Thermal Environment," *ECCOMAS Proceedia*, 2021, pp. 5191–5200. doi: 10.7712/120121.8859.18480.

[46] S.K. Jena, S. Chakraverty, V. Mahesh, and D. Harursampath, "Application of Haar wavelet discretization and differential quadrature methods for free vibration of functionally graded micro-beam with porosity using modified couple stress theory," *Eng. Anal. Boundary Elem.*, vol. 140, pp. 167–185, July 2022, doi: 10.1016/j.enganabound.2022.04.009.

[47] I.M. Nazmul, S. Nahid, and D. Indronil, "Analytical solutions for vibration of Bi-directional functionally graded nonlocal nanobeams," *Res. Eng.*, vol. 18, p. 101046, June 2023, doi: 10.1016/j.rineng.2023.101046.

[48] C.Y. Wang and C.M. Wang, "Exact Vibration Solutions for a Class of Nonuniform Beams," *J. Eng. Mech.*, vol. 139, no. 7, pp. 928–931, July 2013, doi: 10.1061/(ASCE)EM.1943-7889.0000535.

[49] L. Wu, Q. Wang, and I. Elishakoff, "Semi-inverse method for axially functionally graded beams with an anti-symmetric vibration mode," *J. Sound Vib.*, vol. 284, no. 3–5, pp. 1190–1202, June 2005, doi: 10.1016/j.jsv.2004.08.038.

[50] X.-F. Li, Y.-A. Kang, and J.-X. Wu, "Exact frequency equations of free vibration of exponentially functionally graded beams," *Appl. Acoust.*, vol. 74, no. 3, pp. 413–420, Mar. 2013, doi: 10.1016/j.apacoust.2012.08.003.

[51] A.E. Alshorbagy, M.A. Eltaher, and F.F. Mahmoud, "Free vibration characteristics of a functionally graded beam by finite element method," *Appl. Math. Model.*, vol. 35, no. 1, pp. 412–425, Jan. 2011, doi: 10.1016/j.apm.2010.07.006.

[52] A. Shahba, R. Attarnejad, M.T. Marvi, and S. Hajilar, "Free vibration and stability analysis of axially functionally graded tapered Timoshenko beams with classical and non-classical boundary conditions," *Compos. Part B-Eng.*, vol. 42, no. 4, pp. 801–808, June 2011, doi: 10.1016/j.compositesb.2011.01.017.

[53] S. Kukla and J. Rychlewska, "An approach for free vibration analysis of axially graded beams," *J. Theor. Appl. Mech.*, vol. 53, p. 859, July 2016, doi: 10.15632/jtam-pl.54.3.859.

[54] M.A. Mahmoud, "Free vibrations of tapered and stepped, axially functionally graded beams with any number of attached masses," *Eng. Struct.*, vol. 267, p. 114696, Sept. 2022, doi: 10.1016/j.engstruct.2022.114696.

[55] P. Sharma, M. Gautam, and M. Chaturvedi, "Effects of material grading and geometry on natural frequency of functionally graded beam," *Mater. Today-Proc.*, vol. 62, pp. 4222–4224, 2022, doi: 10.1016/j.matpr.2022.04.732.

[56] K. Kondakcıand S.B. Coşkun, "Analysis of the Axial Vibration of Non-Uniform and Functionally Graded Rods via an Analytical-Based Numerical Approach," *Vibration*, vol. 6, no. 4, pp. 876–894, Oct. 2023, doi: 10.3390/vibration6040052.

[57] J. Jędrysiak, "Theoretical Tolerance Modelling of Dynamics and Stability for Axially Functionally Graded (AFG) Beams," *Materials*, vol. 16, no. 5, p. 2096, Mar. 2023, doi: 10.3390/ma16052096.

[58] J.-P. Wang, R.-Y. Ge, and Y. Tang, "Application of Interpolating Matrix Method to Study Dynamics of Axially Moving Beams Made of Functionally Graded Materials," *Appl. Sci.*, vol. 13, no. 3, p. 1449, Jan. 2023, doi: 10.3390/app13031449.

[59] Z. Chun and Z. Zheng, "Three-dimensional analysis of functionally graded plate based on the Haar wavelet method," *Acta Mech. Solida Sin.*, vol. 20, no. 2, pp. 95–102, June 2007, doi: 10.1007/s10338-007-0711-3.

[60] J. Majak, M. Pohlak, K. Karjust, M. Eerme, J. Kurnitski, and B.S. Shvartsman, "New higher order Haar wavelet method: Application to FGM structures," *Compos. Struct.*, vol. 201, pp. 72–78, Oct. 2018, doi: 10.1016/j.compstruct.2018.06.013.

[61] M. Kirs, K. Karjust, I. Aziz, E. Õunapuu, and E. Tungel, "Free vibration analysis of a functionally graded material beam: evaluation of the Haar wavelet method," *Proc. Est. Acad. Sci.*, vol. 67, no. 1, pp. 1–9, Mar. 2018, doi: 10.3176/proc.2017.4.01.

[62] K. Kim, S. Kwak, T. Choe, K. Pang, H. Chae, and D. Yun, "Free Vibration Analysis of Laminated Composite Shells with Varying Thickness Using Haar Wavelet Discretization Method," *J. Vib. Eng. Technol.*, vol. 10, no. 7, pp. 2715–2750, Oct. 2022, doi: 10.1007/s42417-022-00517-9.

[63] M. Mikola, J. Majak, M. Pohlak, and B. Shvartsman, "Higher order Haar wavelet method for vibration analysis of functionally graded beam," *AIP Conf. Proc.*, 2022, vol. 245, p. 380003. doi: 10.1063/5.0081476.

[64] I. Aziz, Siraj-Ul-Islam, and F. Khan, "A new method based on Haar wavelet for the numerical solution of two-dimensional nonlinear integral equations," *J. Computat. Appl. Math.*, vol. 272, pp. 70–80, Dec. 2014, doi: 10.1016/j.cam.2014.04.027.

[65] M. Ratas and A. Salupere, "Application of Higher Order Haar Wavelet Method for Solving Nonlinear Evolution Equations," *Math. Model. Anal.*, vol. 25, no. 2, pp. 271–288, Mar. 2020, doi: 10.3846/mma.2020.11112.

[66] M. Ratas, J. Majak, and A. Salupere, "Solving Nonlinear Boundary Value Problems Using the Higher Order Haar Wavelet Method," *Mathematics*, vol. 9, no. 21, p. 2809, Nov. 2021, doi: 10.3390/math9212809.

[67] L. Kivistik, M. Mehrparvar, M. Eerme, and J. Majak, "Dynamics of flight of the fragments with higher order Haar wavelet method," *PEAS*, vol. 73, no. 2, pp. 108–115, Mar. 2024, doi: 10.3176/proc.2024.2.02.

[68] M. Mehrparvar, J. Majak, K. Karjust, and M. Arda, "Free vibration analysis of tapered Timoshenko beam with higher order Haar wavelet method," *PEAS*, vol. 71, no. 1, pp. 77–83, Feb. 2022, doi: 10.3176/proc.2022.1.07.

[69] S.K. Jena and S. Chakraverty, "Dynamic behavior of an electromagnetic nanobeam using the Haar wavelet method and the higher-order Haar wavelet method," *Eur. Phys. J. Plus*, vol. 134, no. 10, p. 538, Oct. 2019, doi: 10.1140/epjp/i2019-12874-8.

[70] A. Haar, "Zur Theorie der orthogonalen Funktionensysteme," *Math. Ann.*, vol. 69, no. 3, pp. 331–371, Sept. 1910, doi: 10.1007/BF01456326.

[71] R.S. Stanković and B.J. Falkowski, "The Haar wavelet transform: its status and achievements," *Comput. Electr. Eng.*, vol. 29, no. 1, Jan. 2003, doi: 10.1016/S0045-7906(01)00011-8.

[72] H. Saeedi, N. Mollahasani, M. Moghadam, and G. Chuev, "An operational Haar wavelet method for solving fractional Volterra integral equations," *Int. J. Appl. Math. Comput. Sci.*, vol. 21, no. 3, pp. 535–547, Sept. 2011, doi: 10.2478/v10006-011-0042-x.

[73] Ü. Lepik, "Numerical solution of differential equations using Haar wavelets," *Math. Comput. Simul.*, vol. 68, no. 2, pp. 127–143, Apr. 2005, doi: 10.1016/j.matcom.2004.10.005.

[74] C. Cattani, "Haar wavelets based technique in evolution problems," *Proc. Est. Acad. Sci.s. Phys. Math.*, vol. 53, no. 1, p. 45, 2004, doi: 10.3176/phys.math.2004.1.04.

[75] C. Cattani and M. Pecoraro, "Nonlinear differential equations in wavelet bases," *Ŕęóńňč÷íčé âłńíčę*, vol. 3, no. 4, pp. 4–10, 2000.

[76] C.F. Chen and C.H. Hsiao, "Haar wavelet method for solving lumped and distributed-parameter systems," *IEE Proc.-Control Theory Appl.*, vol. 144, no. 1, Jan. 1997, doi: 10.1049/ip-cta:19970702.

[77] H. Hein and L. Feklistova, "Free vibrations of non-uniform and axially functionally graded beams using Haar wavelets," *Eng. Struct.*, vol. 33, no. 12, pp. 3696–3701, Dec. 2011, doi: 10.1016/j.engstruct.2011.08.006.

[78] MathWorks. MATLAB R2020b. Natick, Massachusetts: The MathWorks Inc., 2020 Retrieved from https://www.mathworks.com.

[79] I. Caliò and I. Elishakoff, "Closed-Form Trigonometric Solutions for Inhomogeneous Beam-Columns on Elastic Foundation," *Int. J. Struct. Stab. Dyn.*, vol. 4, no. 1, pp. 139–146, Mar. 2004, doi: 10.1142/S0219455404001112.

[80] J.-C. Hsu, H.-Y. Lai, and C.K. Chen, "Free vibration of non-uniform Euler–Bernoulli beams with general elastically end constraints using Adomian modified decomposition method," *J. Sound Vib.*, vol. 318, no. 4–5, pp. 965–981, Dec. 2008, doi: 10.1016/j.jsv.2008.05.010.